Transient Liquid Phase Bonding of Nickel Superalloys and Stainless Steels: *Modeling and Experimental Investigations*

MUHAMMAD A. ARAFIN

A Thesis

in

The Department

of

Mechanical and Industrial Engineering

Presented in Partial Fulfillment of the Requirements
for the Degree of Master of Applied Science (Mechanical Engineering) at
Concordia University
Montreal, Quebec, Canada.

August, 2006

© Muhammad A. Arafin, 2006

Library and Archives Canada

Published Heritage Branch

395 Wellington Street
Ottawa ON K1A 0N4
Canada

Bibliothèque et Archives Canada

Direction du Patrimoine de l'édition

395, rue Wellington
Ottawa ON K1A 0N4
Canada

Your file Votre référence
ISBN: 978-0-494-20757-4
Our file Notre référence
ISBN: 978-0-494-20757-4

NOTICE:
The author has granted a non-exclusive license allowing Library and Archives Canada to reproduce, publish, archive, preserve, conserve, communicate to the public by telecommunication or on the Internet, loan, distribute and sell theses worldwide, for commercial or non-commercial purposes, in microform, paper, electronic and/or any other formats.

The author retains copyright ownership and moral rights in this thesis. Neither the thesis nor substantial extracts from it may be printed or otherwise reproduced without the author's permission.

AVIS:
L'auteur a accordé une licence non exclusive permettant à la Bibliothèque et Archives Canada de reproduire, publier, archiver, sauvegarder, conserver, transmettre au public par télécommunication ou par l'Internet, prêter, distribuer et vendre des thèses partout dans le monde, à des fins commerciales ou autres, sur support microforme, papier, électronique et/ou autres formats.

L'auteur conserve la propriété du droit d'auteur et des droits moraux qui protège cette thèse. Ni la thèse ni des extraits substantiels de celle-ci ne doivent être imprimés ou autrement reproduits sans son autorisation.

In compliance with the Canadian Privacy Act some supporting forms may have been removed from this thesis.

While these forms may be included in the document page count, their removal does not represent any loss of content from the thesis.

Conformément à la loi canadienne sur la protection de la vie privée, quelques formulaires secondaires ont été enlevés de cette thèse.

Bien que ces formulaires aient inclus dans la pagination, il n'y aura aucun contenu manquant.

ABSTRACT

Transient Liquid Phase Bonding of Nickel Superalloys and Stainless Steels: Modeling and Experimental Investigations

Muhammad A. Arafin

A combination of direct experimentation and computational modeling approach was used to predict the isothermal solidification times during the *Transient Liquid Phase (TLP) Bonding* of nickel superalloys, Inconel 718 and 625, and stainless steels, 410 and 321, with nickel based filler alloy, BNi-2. Unlike conventional modeling, the diffusion of solute atoms was modeled by the *Random Walk Modeling* technique which can take into account the physical and chemical uncertainties associated with the *TLP Bonding* experiments. The model equations for migrating solid/liquid interface and solute distribution have been modified and presented in this thesis.

Cumulative probability distributions and probability density functions of isothermal solidification times were calculated for different process conditions and compared with experimental data. Good agreement was observed when nickel superalloys and SS 321 were used as base alloys. However, it was found that both models, based on the assumption of 0.3 at% solubility of boron, underestimated the isothermal solidification time requirement for SS 410/BNi-2 at higher bonding temperatures due to the decreased boron solubility. Excellent agreement was observed when 0.2 at% boron solubility was used. Isothermal solidification times predicted by silicon diffusion model based on the EDS analyses were also in good agreement with the experimental data for this combination.

Acknowledgement

I would like to express my heart-felt gratitude to my thesis supervisors Dr. Medraj and Dr. Bocher for their continuous guidance, support and encouragement throughout the course of this thesis.

I would also like to thank Prof. René LeGall at Université Polytechnique de Nantes (France) for helpful discussions and accessibility to EDS equipment and both CRIAQ (Center for Research and Innovation in Aerospace in Quebec) and Pratt & Whitney Canada for financial support to conduct this research.

Finally, I would like to thank my wife Sharmin for her love, tolerance, encouragement and valuable suggestions, my parents and brothers for their kind support and inspirations. Last but not the least; I would like to thank all our group members for their cooperation and valuable feedback.

Table of Contents

List of Figures viii

List of Tables xii

Chapter 1: Introduction 1

1.1 Brazing 2

1.2 Nickel Based Brazing Filler Metals 4

1.3 Brazing Process Variables 6

1.3.1 Surface Preparation 7

1.3.2 Joint Gap 7

1.3.3 Brazing Temperature and Holding Time 7

1.4 Limitations of Brazing 8

1.5 Transient Liquid Phase (TLP) Bonding 10

1.5.1 Advantages of TLP Bonding 11

1.5.2 Limitations of TLP Bonding 12

1.6 Objectives of this Research 14

Chapter 2: Literature Survey 16

2.1 TLP Stages 16

2.2 Modeling of TLP Bonding 20

2.2.1 Base Metal Dissolution 20

2.2.2 Isothermal Solidification 22

2.2.3 Homogenization 33

Chapter 3: Scopes of Present Investigations 34

Chapter 4: Experimental Procedures 37

4.1 Materials 37

4.2 Wedge-Gap Specimens and Brazing Procedures 37

Chapter 5: Microstructures of the Joint and Related Measurements 40

5.1 Microstructures of the Brazed Joints 40

5.1.1 Inconel 718/BNi-2 and Inconel 625/BNi-2 42

5.1.2 SS 410/BNi-2 and SS 321/BNi-2 49

5.2 Diffusion Induced Precipitations 56

5.3 Dissolution of Base Alloys 57

5.4 Maximum Brazing Clearances and Isothermal Solidification Times 58

Chapter 6: Mathematical Modeling and Methodology 60

6.1 Random Walk Modeling Based on Migrating Solid/Liquid Interface 60

6.1.1 Calculation of Diffusion Coefficients 61

6.1.2 Modified Model Equations 61

6.2 Random Walk Modeling Based on Solute Distribution Law 63

6.3 Summary of the Proposed Methodology 64

Chapter 7: Results and Discussions: 65

7.1 Inconel 718/BNi-2 and Inconel 625/BNi-2 65

7.1.1 Migrating Solid/Liquid Interface Model 65

7.1.2 Solute Distribution Model 70

7.2 SS 410/BNi-2 and SS 321/BNi-2 72

7.2.1 Migrating Solid/Liquid Interface Model 72

7.2.2 Solute Distribution Model 78

7.2.3 Silicon Diffusion Model for SS 410/BNi-2 79

Chapter 8: Summary and Conclusions 81

8.1 Summary and Conclusions 81

8.2 Contributions 83

8.3 Future Research Directions 84

References 86

List of Figures

Fig. 1.1	Schematic of typical brazing process	2
Fig. 1.2	Typical centerline eutectic microstructure of an Inconel 718/BNi-2 brazed joint	10
Fig. 1.3	SEM micrograph of an Inconel 625/BNi-2 joint showing complete isothermal solidification	11
Fig. 2.1	Nominal stages of TLP bonding process	17
Fig. 2.2	Relation between (a) holding time and the dissolution parameter and (b) ln(K) and 1/T	21
Fig. 2.3	Schematic diagram showing solute distribution during the isothermal solidification stage in TLP bonding	24
Fig. 2.4	Eutectic width vs. square root of holding time	27
Fig. 2.5	$t_f^{1/2}$ vs. $(2h/D^{1/2})$ plot to determine J of equation (2.17)	32
Fig. 4.1	The wedge shape joint gap specimen	39
Fig. 5.1	Typical microstructure of a brazed joint showing three distinct areas	41
Fig. 5.2	Microstructures of the Inconel 718/BNi-2 joint brazed at 1394K for various lengths of times: (a) 10 min, (b) 20 min, (c) 30 min and (d) 50 min.	43
Fig. 5.3	Microstructures of Inconel 718/BNi-2 joints brazed at 1325K for 70 minutes with initial joint gaps of (a) ≈ 60 μm and (b) ≈ 100 μm	44
Fig. 5.4	Microstructures of Inconel 625/BNi-2 joints brazed for 30 minutes at (a) 1358K and (b) 1394K	45

Fig. 5.5 (a) SEM micrograph of Inconel 625/BNi-2 joint brazed at 1325K for 10 minutes showing centerline eutectics, (b) EDS number of counts versus the measurement step (0.5 μm) 46

Fig. 5.6 Optical micrograph of Inconel 625/BNi-2 joint showing the centerline eutectic morphology 48

Fig. 5.7 (a) SEM micrograph of SS 410/BNi-2 joint brazed at 1394K for 50 minutes showing centerline eutectics, (b) and (c) EDS analyses 52

Fig. 5.8 (a) SEM micrograph of SS 410/BNi-2 joint brazed at 1325K for 50 minutes showing centerline eutectics, (b) and (c) EDS analyses 53

Fig. 5.9 Microstructure of a SS 321/BNi-2 joint brazed at (a) 1394K and (b) 1325K, for 10 minutes showing centerline eutectics 54

Fig. 5.10 Line scans through the centerline eutectics of an SS 410/BNi-2 joint brazed at 1325K for 50 minutes 55

Fig. 5.11 Effect of bonding temperature and time on dissolution thickness of Inconel 718 base alloy for an initial joint gap of 75 μm 57

Fig. 5.12 Micrograph showing the initiation of brittle eutectic phase (Inconel 718/BNi-2 joint brazed at 1394K for 50 minutes) 58

Fig. 5.13 Effect of holding time and temperature on the maximum brazing clearances for (a) Inconel 718/BNi-2, (b) Inconel 625/BNi-2, (c) SS 410/BNi-2 and (d) SS 321/BNi-2 combination 59

Fig. 6.1 Flow chart illustrating the methodology of the current study 64

Fig. 7.1 Example of normality check of diffusion coefficient being calculated for Inconel 625/BNi-2 combination for 1325K bonding temperature 67

Fig. 7.2 Cumulative probability plot and probability density plot of isothermal solidification time (migrating solid/liquid interface model) for (a) Inconel 718/BNi-2 and (b) for an initial joint gap of 75 μm and 1358K bonding temperature 68

Fig. 7.3 Comparison of predicted isothermal solidification times with different confidence levels (migrating solid/liquid interface model) with experimental data for an initial joint gap of 75 μm for (a) Inconel 718/BNi-2 and (b) Inconel 625/BNi-2 69

Fig. 7.4 Model verification for 85 μm joint gap at 1358K: (a) Inconel 718/BNi-2 and (b) Inconel 625/BNi-2 70

Fig. 7.5 Comparison of predicted isothermal solidification times with different confidence levels (solute distribution model) with experimental data for an initial joint gap of 75 μm for (a) Inconel 718/BNi-2 and (b) Inconel 625/BNi-2 71

Fig. 7.6 Cumulative probability plot and probability density plot of isothermal solidification time for (a) SS 410/BNi-2 and (b) SS 321/BNi-2 for an initial joint gap of 70 μm and 1325K bonding temperature 74

Fig. 7.7 Comparison of predicted isothermal solidification times with different confidence levels (solute distribution model) with experimental data for an initial joint gap of 70 μm for (a) SS 410/BNi-2 and (b) SS 321/BNi-2 75

Fig. 7.8 Verification of decreased solubility (0.2 at%) for SS 410/BNi-2 combinations with an initial joint gap of 70 μm for (a) 1358K and (b) 1394K 76

Fig. 7.9 Verification of decreased boron solubility for for SS 410/BNi-2 at 1358K with an initial joint gap of 80 μm: (a) 0.3 at% and (b) 0.2 at% (SS 410/BNi-2 at 1358K) 76

Fig. 7.10 Verification of 0.3 at% boron solubility for SS 321/BNi-2 combination for an initial joint gap of 80μm at 1358K 77

Fig. 7.11 Comparison of predicted isothermal solidification times with different confidence levels (solute distribution model) with experimental data for an initial joint gap of 70 μm for (a) SS 410/BNi-2 and (b) SS 321/BNi-2 78

Fig. 7.12 Verification of 0.2 at% solubility limit for SS 410/BNi-2 combination for 1394K bonding temperature with an initial joint gap of 70 μm 79

Fig. 7.13 Comparison of predicted isothermal solidification times with different confidence levels (silicon diffusion model based on solute distribution law) with experimental data for an initial joint gap of 70 μm for SS 410/BNi-2 80

List of Tables

Table 4.1 Nominal compositions of Inconel 625, Inconel 718, SS 410, SS 321 and BNi-2 38

Table 4.2 Braze tests matrix 39

Table 7.1 Range of diffusion coefficients obtained from experimentally determined isothermal solidification times for Inconel 718/BNi-2 combination 66

Table 7.2 Range of diffusion coefficients obtained from experimentally determined isothermal solidification times for Inconel 625/BNi-2 combination 66

Table 7.3 Range of diffusion coefficients obtained from experimentally determined isothermal solidification times for SS 410/BNi-2 combination 72

Table 7.4 Range of diffusion coefficients obtained from experimentally determined isothermal solidification times for SS 321/BNi-2 combination 72

Chapter 1

Introduction

Inconel 625 and 718 are extremely versatile austenitic nickel based superalloys with excellent strength and good ductility at very high temperature [1]. Typical applications include aero-engine hot section components, miscellaneous hardware, tooling and liquid rocket components involving cryogenic temperatures. However, like other austenitic nickel based superalloys that contain a substantial amount of Ti and Al, they are highly susceptible to the heat affected zone cracking during welding [1,2].

SS 410 is martensitic stainless steel that provides good corrosion resistance plus high strength and hardness [3]. Typical applications include steam and gas turbine parts, pump and valve shafts, miscellaneous hardware, tooling and petroleum fractionating towers. However, due to hardenability, it is also highly susceptible to the heat affected zone cracking during welding [3].

Austenitic stainless steel 321, stabilized with titanium, is widely used in applications such as gas turbines, heat exchangers, steam and hot gas valves, steam generators, expansion joints, super-heaters and re-heaters etc. due to its high strength, ductility, good resistance to creep and to oxidation damage at elevated temperatures [4]. However, many intergranular cracks have been observed near welds, generally in the heat affected zone (HAZ) of thick components or of attachment welds. This form of cracking

is generally referred to as reheat cracking and is associated to relaxation of residual stresses due to welding [4,5].

Typical high temperature brazing with nickel based fillers evolved as an effective way to join nickel superalloys and stainless steels [2,7]. It has the capability of producing oxidation and corrosion resistant, high strength joints suitable for elevated temperature applications [2,6-8].

1.1 Brazing:

Brazing comprises a group of joining processes in which coalescence is produced by heating to suitable temperatures above 450°C using a filler metal that must have a liquidus temperature below the solidus temperature(s) of the base metal(s) and above 450°C [8,9]. At the brazing temperature the filler metal is distributed between the closely fitted surfaces of the joint by capillary attraction, interacts with a thin layer of the base metal and when cooled to room temperature exceptionally strong and sealed joints are formed due to grain structure interactions as shown in Fig. 1.1 [10].

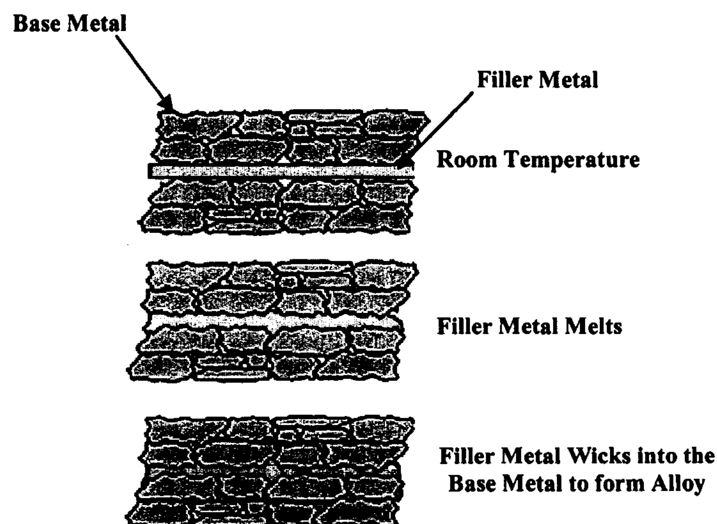

Fig. 1.1 Schematic of typical brazing process [10]

In *brazing*, it is not always easy to achieve complete wetting of the component surfaces and when it does occur, the resulting alloying between the filler and the base metal components can cause excessive erosion of the parent materials, embrittlement of joints due to the formation of brittle intermetallic phases, and other undesirable effects such as porosity, cracks etc.[10,11]. Thereafter, due to presence of the lower melting point filler metals, the upper working temperature of the assembly is also considerably reduced [9,11]. However, not withstanding these problems, brazing can be used to fill joints of irregular dimensions and to produce well-rounded fillets at the edges of the joint [11].

There exists a joining technique, known as *diffusion bonding*, which eliminates the need for wetting and spreading by a filler metal [8,11]. It is a solid state joining process for the fabrication of metal-metal, ceramic-ceramic and ceramic-metal joints that is conceptually simple because the process requires no localized melting of components or introduction of foreign bonding materials but merely that mating surfaces are brought into intimate, atomic scale contact so that an interface can be formed by interdiffusion to create a structural continuum [8]. Although the formation of intermetallic phases can also occur in *diffusion bonding*, it is easier to select a safe combination of materials because only fewer constituents are involved and, once formed, the joints become stable to high temperature so that the service temperature of the assembly can actually exceed the temperature of the joining without risk of re-melting [11]. However, its application is limited because it not possible for the joints with variable width and the quality of the joints is highly dependent on the surface cleanliness [8]. Moreover, high loads, typically 10 to 100 MPa needs to be applied during the bonding cycle to ensure good contact

across the joint interface, the duration of heating cycle, typically several hours compared with seconds in brazing because solid state diffusion is much slower than wetting of a solid by a liquid, and, also, the absence of any significant fillets to minimize the stress concentrations at the edges of joints significantly limit the application of this solid state joining technique [11].

1.2 Nickel Based Brazing Filler Metals:

Nickel based brazing fillers containing boron, silicon or phosphorus as melting point depressants can produce joints with higher temperature capabilities and improved mechanical properties, such as ductility, corrosion resistance etc., compared to traditional silver and copper based filler metals [6,12]. The metallurgical basis for these filler metals was derived from nickel based hard facing alloys [12]. The melting point of pure nickel is 1455°C [13]. This temperature is much higher than the melting points of most base metals. However, according to the definition of brazing, base metals must be joined together at a brazing temperature below their melting points [9]. Therefore, to braze with nickel filler metals, elements must be alloyed with the nickel to lower its melting point below that of most base metals. The alloying elements in nickel based filler alloys serve different purposes and are optimized differently although there are some similarities in compositions [12]. Some of these important elements are as follows:

Boron (B) and Silicon (Si): Both boron and silicon are strong melting point depressants, e.g. when alloyed with nickel, individually, mere 3.6 wt% boron and 11.8 wt% silicon will lower the melting point to 1093°C and 1125°C, respectively [13]. The lower melting point allows the use of nickel-boron or nickel-silicon filler metals to braze a wide range of metals at temperature far below their melting points. Although boron and

silicon significantly lower the melting points of the nickel based filler metals, binary nickel-boron or nickel-silicon alloys suffer from many shortcomings, such as low tensile strength, higher hardness, low corrosion resistance and excessive fluidity when molten [12]. Thus, binary nickel-boron or nickel-silicon brazing filler metals are not commercially available and additional elements are alloyed to obtain the desired physical properties.

Ni-B-Si: When boron and silicon are alloyed together in nickel with 1.5-3.5% boron and 2.75-4.0% silicon, suitable brazing filler metal can be formed with a melting point as low as 1040°C and 1055°C [13]. The addition of Si was found to increase the corrosion resistance of the assembly [14].

Phosphorus (P): Phosphorus also acts as a melting point depressant. It reduces the melting point of nickel to 870°C from 1455°C [15]. However, unlike boron and silicon, phosphorus does produce satisfactory brazing filler metal when alloyed alone with nickel [12]. In spite of having some satisfactory brazing characteristics and an extremely low melting point, binary Ni-P filler metal has some disadvantages such as low strength, ductility and greater fluidity when molten [12,16].

Chromium (Cr): Chromium is well known to add strength and corrosion resistance. In order to maximize the benefit of the Cr addition, the time at brazing temperature should be long enough to allow boron to diffuse out of the braze joint and into the base metal because the loss of boron will result in a strong, corrosion resistant braze joint with a melting point higher than the original filler metal [12]. BNi-5 (Ni-Si alloyed with 19 wt% Cr) is one of the strongest corrosion resistant filler metals used extensively for high temperature applications [7]. Another example is BNi-7 which is a

Ni-P based filler alloyed with 13 wt% Cr [12]. This commercially available filler alloy was found to have some extremely satisfactory brazing characteristics such as increased molten viscosity, more strength and ductility and corrosion resistance [17].

Ni-B-Cr-Si: By adding all three elements to pure nickel, alloy with melting point at 1000°C can be formed and, if the holding time at brazing temperature is long enough to diffuse most of the boron into the base alloy, extremely satisfactory brazed joint with high strength, enhanced corrosion resistance can be obtained [12,18].

Copper (Cu), Tungsten (W) Molybdenum (Mo) and Iron (Fe): Cu is usually alloyed with *Ni* and *Cr* to increase the corrosion resistances of the brazed joint, especially in saltwater environments and aqueous media; *W* reduces viscosity during brazing by elevating the melting point of the filler alloy and thereby increases the high temperature strength of the diffusion brazed joint; *Mo* serves the purpose of increasing the viscosity of brazing filler metals, adds high temperature strength and, when alloyed with *Cr* and *Cu*, enhances corrosion resistances to aqueous media [12,19]. In addition to boron and/or silicon, sometimes *Fe*, generally considered to be a neutral element, is inadvertently alloyed with nickel based filler metals; however, it does impart some ductility [12,20].

1.3 Brazing Process Variables:

In addition to the base and filler alloy characteristics, the other process variables that contribute to the structure and properties of a diffusion brazed joint are discussed as follows:

1.3.1 Surface Preparation:

Surface preparation plays a very significant role during brazing process because in order to ensure complete wetting of liquid braze on the base metal surface, high surface tension, low contact angle and low viscosity are required. The flow of the molten brazing filler metal is facilitated by capillary action, which in turn results from surface energy effect [19,21-24,26]. A clean surface is, therefore, absolutely vital for wetting, flow and filling of cracks and small cavities by the liquid filler alloy during the brazing cycle [10]. A clean surface can be obtained by either or combination of the several treatments such as grinding, grit blasting, hydrogen gas cleaning, vacuum cleaning, fluoride ion cleaning, nickel/gold flash etc. [2,22,25,26].

1.3.2 Joint Gap:

The initial joint gap size has a very significant role in the kinetics of diffusion of melting point depressants into the base metal during brazing and as a result on the final brazed joint microstructures because the wider the joint gap, the more the amount of filler alloy that contains the melting point depressants such as boron and silicon which in turn would require longer time to form a isothermally solidified joint which is free of deleterious brittle eutectic phases [7,27].

1.3.3 Brazing Temperature and Holding Time:

Brazing temperature has a strong influence on wetting, dissolution of base metal and diffusion of melting point depressants into the base alloy [2,7,26-29]. According to the process requirement, it has to be above the liquidus temperature of the filler alloy

being used and below the solidus temperature of the base alloys [8,9]. Higher brazing temperature reduces the isothermal solidification time requirement since the diffusivities of melting point depressants increase with temperature [2]. There are other beneficial aspects such as: (a) annealing, stress relief or heat treatment of the base alloy are combined with brazing, (b) surface impurities and oxides can be removed by vacuum brazing, (c) higher melting but more economical and efficient brazing alloy can be used and (d) base metal and filler alloy interactions are being promoted in order to modify composition and microstructure of the brazed joint [26]. However, sometimes lower brazing temperature is chosen to (a) minimize the heat affects on the base metal thus avoiding grain growth, (b) economize the heating expenditures, (c) reduce the dissolution of base alloy which is very important during brazing of thin wall structural components etc. [21,26,29]

Since diffusion is a time dependent process, holding time plays the most significant role for a given brazing temperature [7,18,30,31]. It should be long enough to allow the melting point depressants to diffuse out into the base alloy and, thus, the formation of brittle eutectic phases can be avoided.

1.4 Limitations of Brazing:

Following are the common problems encountered when superalloys and stainless steels are brazed:

1. *Melt-back:* As the melting point depressing element diffuses into the base alloy, it reaches a high enough concentration near the interface to cause localized melting of the base metals and, thus, reduces the effective thickness of the ductile base

metal which is of great concern when thin material is brazed or when brazed joint must withstand vibration or impact load [26,29].

2. *Porosity:* Pores and partially filled cracks often form in brazed joints as a result of oxide residues and contaminants not completely eliminated by thermo-chemical cleaning and other surface preparation techniques [10,26]. This effectively reduces the integrity of the brazement. In addition to non-wetting, due to improper cleanliness and mating of surfaces, shrinkage of the braze on solidification often lead to the formation of porosity [32]. Besides, the difference in chromium concentrations between the filler and the base metal can lead to the formation of Kirkendall porosity after post-brazing annealing treatment [33].
3. *Grain size:* The optimum grain size structure of a brazed joint is often one of large grains filling the whole width of the joint area; however, solidification may also result in a continuous grain boundary running along the center of the braze which is undesirable for high temperature applications [26].
4. *Second phase precipitates:* Nickel based brazing filler metals containing boron and/or silicon are commonly used to join nickel superalloys and stainless steels [6,7,18]. However, these melting point depressants form eutectic structures, as shown in Fig. 1.2, which are extremely hard and contain very brittle intermetallic compounds (borides, phosphides and silicides) with nickel and chromium which are detrimental to the mechanical properties of brazed joint [6,7,34].

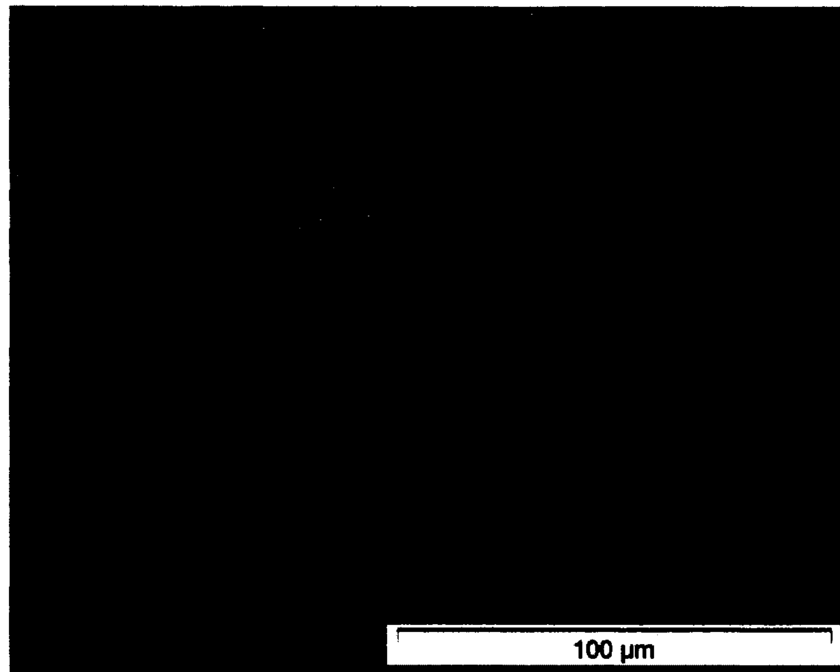

Fig. 1.2 Typical centerline eutectic microstructure of an Inconel 718/BNi-2 brazed joint

1.5 Transient Liquid Phase (TLP) Bonding:

There exists a hybrid joining process which can prevent the formation of the abovementioned deleterious phases [9,11]. It is known as *Transient Liquid Phase (TLP) Bonding*, alternatively termed as *Diffusion Brazing* [27,35]. The *TLP Bonding* process uses a low melting filler alloy to wet the contacting base material and that subsequently solidifies isothermally via a fast diffusing element, e.g. boron [36]. Unlike conventional brazing, the thermal exposure used for the *TLP Bonding* cycle is long enough to induce complete isothermal solidification at the bonding temperature and thus, the formation of eutectic phases is avoided during cooling [2,11,36], an example is shown in Fig. 1.3.

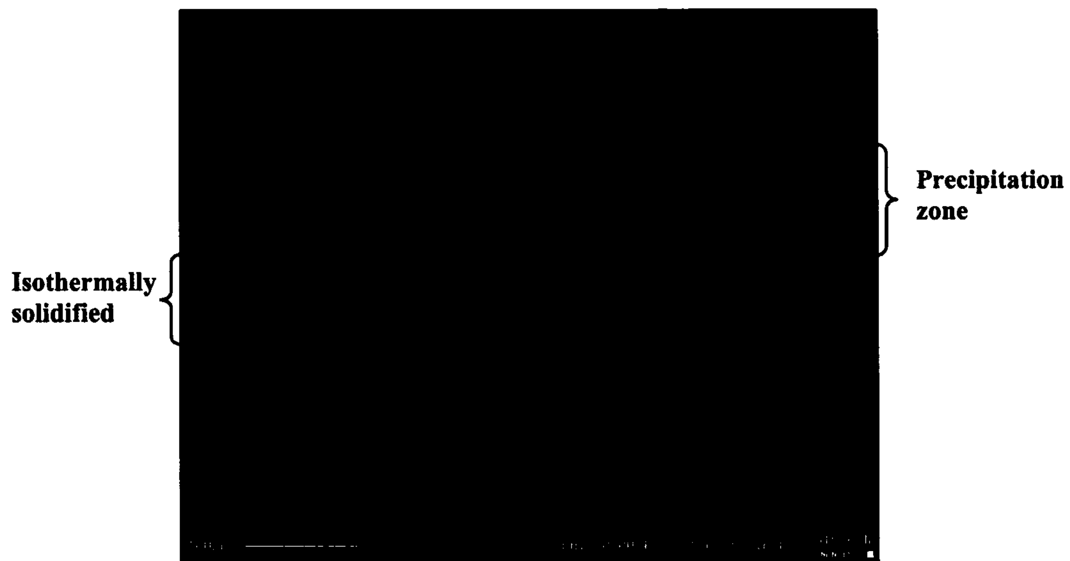

Fig. 1.3 SEM micrograph of an Inconel 625/BNi-2 joint showing complete isothermal solidification

1.5.1 Advantages of TLP Bonding:

TLP Bonding has been employed in a wide range of applications since it has the capability to produce joints that have microstructural and hence mechanical properties similar to that of the base metal [15,18]. Following are some of the major advantages of *TLP Bonding*:

1. Since the bonding temperature is below the solidus of the base metal, joint formation depends on an isothermal, relatively low temperature bonding mechanism [36].
2. Theoretically, no interface remains for the *TLP Bonded* joints [21,37].
3. Wide gap TLP bonding technique permits repair of defects up to 0.1 mm wide [38,39]. The joint preparation before TLP bonding is simple since joining depends on capillary filling [36].

4. Unlike diffusion bonding, the joining process is relatively more tolerant to the presence of a faying surface oxide layer [11,36,40]. For this reason, and because of the absence of thermal stresses, TLP bonding is ideal when joining intermetallic base materials which have stable oxide surface films, high sensitivity to microstructural changes, and poor low temperature ductility [41].
5. The bonding process is ideally suited for joining dissimilar materials and materials which are inherently susceptible to hot cracking or post weld heat treatment cracking problems [2,4,5,42].
6. The bonding process is highly suitable for large and complex shaped components [43].

TLP Bonding has been employed when joining: nickel base and iron base superalloys [39,44-55], titanium base alloys [56-58], stainless steels [18,25], aluminum [59], aluminum base and titanium base metal matrix composites [60-63], copper to austenitic stainless steels [64], and micro-circuitry components [65]. Non-metals have also been joined using *TLP Bonding*; for example, silicon nitride has been bonded at 1550°C using an oxynitride glass [66]. However, in this case the key requirement is that the glass composition must be selected so that thermal expansions mismatch is minimized [43].

1.5.2 Limitations of TLP Bonding:

Although *TLP Bonding* is an excellent bonding technique, the time required to complete isothermal solidification is usually long enough to discourage their potential

applications in many industries [2,18]. Therefore, a thorough understanding of the effect of other process variables, such as bonding temperature and joint gap, on the time required to complete isothermal solidification, is absolutely imperative to reduce the time requirement and thus to optimize the process [7].

Boron containing interlayers are unsuitable for joining nuclear reactor components due to the high neutron absorption cross section of boron [17,67,68]. In this case, nickel base alloys such as *Ni-Cr-Si* or *Ni-Cr-P* can be used although use of these materials does entail some compromises [69,70]. The bonding temperature for *Ni-Cr-Si* alloy is above the solution treatment temperature and so bonding has to be performed before heat treatment [71]. *Palladium* can also be used as melting point depressant [72]. The use of *phosphorus* suffers from a low solubility in nickel [15], as in the case of *boron* [13], but its diffusion coefficient is much smaller than that of *boron* [2,15,18,21].

TLP Bonding and *diffusion bonding* are capable of producing joints that are similar to the parent metals in terms of microstructures and mechanical properties; however, autogeneous *diffusion bonding* has the advantage over *TLP Bonding* that no compositional change is made at the bond line [11,15,18,21]. When nickel based solid solution forming filler alloys are used for *TLP Bonding*, the resulting bond line is much softer than the bulk [73]. Conversely, the formation of brittle intermetallic phases at the bond line due to incomplete isothermal solidification is the major concern for *TLP Bonding* [6,7,74-76]. Both mechanical properties and environmental resistances of the joint can be affected by the compositional changes at the bond line, e.g., when nickel based superalloys and stainless steels are *TLP Bonded*, using *boron* containing interlayers, some *borides* almost invariably remain at the end of the bonding process

[2,17,18,25,27]. If the joint is subsequently re-coated using diffusion coating, these *borides* will tend to become incorporated in the coating which has a highly detrimental effect on its oxidation resistance. The formation of *chromium rich boride* phases can also lead to a sensitization type of corrosion cracks during *TLP Bonding* of austenitic stainless steels [21,77].

1.6 Objectives of this Research:

By a combination of direct experimentation with computational modeling, the optimum joining parameters, such as joint gap, bonding temperature and holding time can be set prior to actual field trials. Although Inconel 625, Inconel 718, SS 410 and SS 321 are the most commonly used alloys in aerospace industry and also in many other applications, modeling studies and experimental investigations of isothermal solidification during *TLP Bonding* of the abovementioned alloys with a nickel based filler alloy, such as BNi-2, could not be found in the literature. It is also worth mentioning that current industrial brazing practice, especially in aerospace industry, for the abovementioned nickel superalloys and stainless steels is using Palnicro-36M filler alloy which is extremely expensive compared to BNi-2 and recently the industry is hoping to replace this costly filler with almost twenty times less expensive BNi-2 because of its promising feedback in terms of producing comparable brazed joints. One of the most important features to look at is the isothermal solidification behavior of this filler with these base alloys and to study the effect of process variables on the time requirement to complete isothermal solidification.

Therefore, a research project was designed to study the kinetics of isothermal solidification during *TLP Bonding* of nickel superalloys, Inconel 718 and 625, and stainless steels, SS 410 and 321, with nickel based filler alloy, BNi-2, in order to predict the time required to complete isothermal solidification and to study the effect of process variables, such as bonding temperature and joint gap, using different mathematical modeling techniques, and to verify the predicted values with experimental investigations. The advantages and shortcomings of the existing modeling approaches have been discussed and, unlike conventional modeling, the diffusion of solute atoms has been modeled using Random Walk Modeling technique which can take into account the physical and chemical uncertainties associated with transient liquid phase bonding experiments. The model equations to determine isothermal solidification time have been modified and presented in this dissertation.

Chapter 2

Literature Survey

The following literature survey is based on the current research performed on the *TLP Bonding* stages and modeling of these stages. The stages of standard *TLP model* will be described along with the assumptions and shortcomings. The existing modeling approaches for different stages of *TLP Bonding* will be critically reviewed and discussed.

2.1 TLP Stages:

Gale and Butts [21] illustrated the *TLP Bonding* stages, as shown in Fig. 2.1, which involves substrates of material A bonded with an interlayer consisting of *A*, plus a melting point depressant *B*. The stages described in [21] are generally well accepted as the major *TLP Bonding* sequences and cited below within the quotation marks:

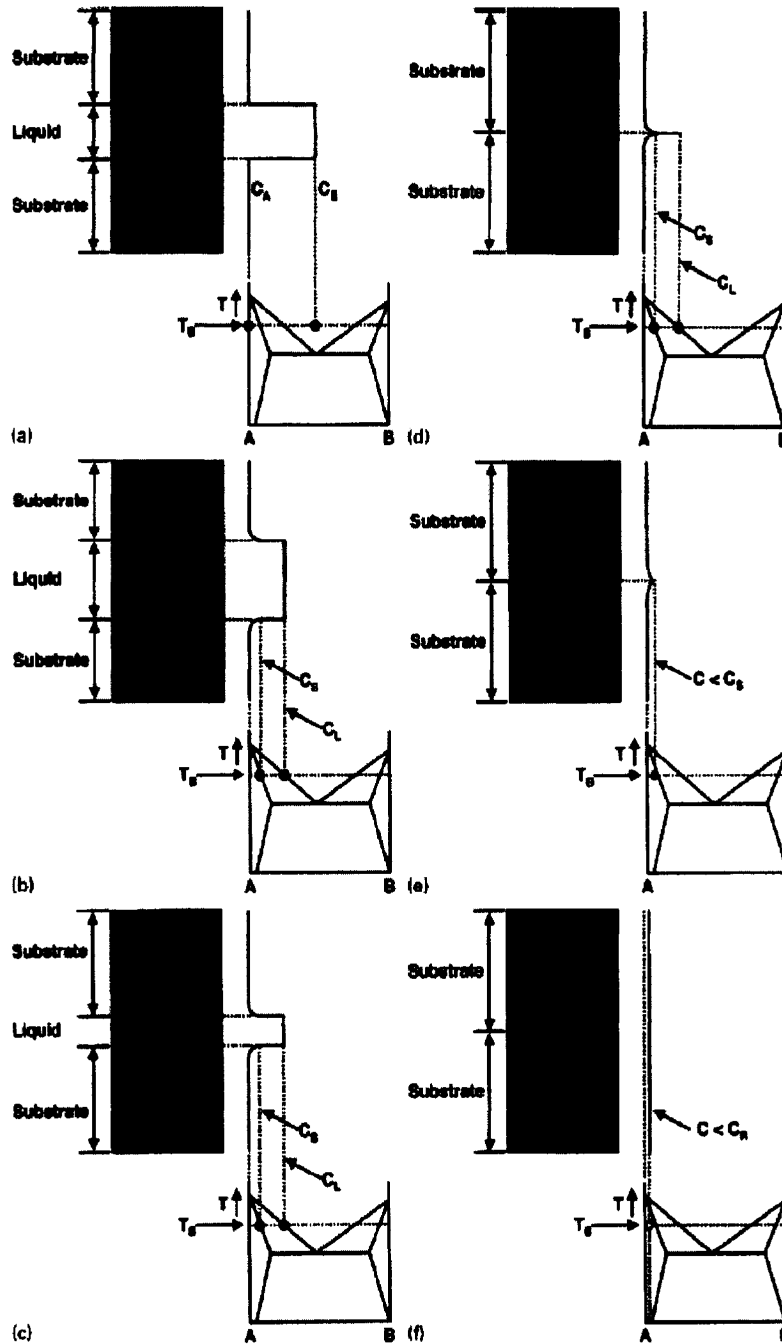

a initial condition; *b* dissolution; *c* isothermal solidification; *d* completion of isothermal solidification; *e* solid state homogenisation; *f* final condition

Fig. 2.1 Nominal stages of *TLP Bonding* process [21]

"The composition of *A-B* interlayer is chosen such that a eutectic melting occurs at the boding temperature (T_B). In such systems three distinctly different processes namely, substrate dissolution, isothermal solidification and solid state homogenization will occur after eutectic melting of the filler.

Substrate Dissolution: Partial dissolution of the substrate material adjusts the composition of the liquid to that of the liquidus (C_L) at T_B. If the composition of the solid immediately adjacent to the liquid is brought to that of the solidus (C_S) at T_B, then the net result will be that local equilibrium is established at the solid/liquid interface. ...Dissolution does not require long range diffusion in the solid and consequently, the activation energy for dissolution is usually very low [78], when compared to that for the interstitial diffusion, let alone substitutional or self diffusion [79]....

Isothermal Solidification: After completion of the dissolution process, the melting point depressant (*B* in the present example) begins to diffuse into the solid substrates. In all standard *TLP process* models, local equilibrium is maintained at the solid/liquid interface throughout the isothermal solidification and so the compositions of the liquid and adjacent solid remain fixed at C_L and C_S, respectively. Thus, as *B* continues to diffuse the liquid narrows during holding at T_B. Given a sufficiently protracted hold at T_B, the liquid will be removed entirely. Isothermal solidification requires long range diffusion in the solid phase and in general, it is much slower than the substrate dissolution stage [28]. However, the time taken to complete isothermal solidification is highly system specific, since this depends on the diffusion coefficient of *B* in *A*, as well as the amount of solute *B* that must be diffused into A which in turn is determined by the composition and thickness of the interlayer....

Solid State Homogenization: Following the composition of isothermal solidification, continued holding at T_B is required to allow homogenization of the remaining solute. The centerline composition of B at T_B must be reduced to below the room temperature solubility of B in A (C_R) if the precipitation of undesired second phase is to be avoided on cooling. As with isothermal solidification, the solid state homogenization requires long range diffusion of the melting point depressant in the substrates [37] and so the rate of this process depends on the value of diffusion coefficient of *B* in *A* at T_B. If there is large difference between C_S and C_R, the solid state homogenization stage can be protracted, even if the diffusion coefficient of *B* in *A* is relatively high....

All standard models of the *TLP process* assume that these three processes are sequential and cannot occur in parallel [43]. This is an important assumption; as it implies that the formation of undesired second phase (e.g. borides) cannot occur at T_B and any such phases must precipitate either before complete melting of the interlayer, and/or on cooling. The universal applicability of this assumption is open to question. The idealized TLP bonding stages described above assumed a eutectic formation system, however, not all TLP interlayers are eutectic formers. Some additional complications in real world *TLP bonds* include:

1. Solid state diffusion during heating to the bonding temperature."
2. Substrates that cannot be approximated to semi-infinite media (fast moving melting point depressants can diffuse right across thin-walled, e.g. honeycomb, substrates during bonding)." [21]

Niemann and Garret [80] joined *Al-B* composite based material using thin copper foils. When the heating rate between room temperature and the eutectic temperature was very slow, insufficient liquid formed at the bonding temperature due to the diffusion of copper into the base metal during the heating stage, and as a result, very poor joint was produced [80]. Based on this result, Macdonald and Eager [81] proposed that a further stage should be included in *TLP Bonding* in order to account for solute diffusion during the heating cycle to the bonding temperature. Another factor that plays a significant role on the kinetics of *TLP Bonding* is the heating rate between the eutectic temperature and the bonding temperature since solute diffusion in the temperature range from the filler metal melting point to the bonding temperature may allow solidification to occur before the selected bonding temperature is reached [82]. Nakagawa *et al.* [82] took this factor into consideration during *TLP Bonding* of Nickel 200 base metal using Ni-19P at% filler. Solidification was found to be occurred when the heating rate was very slow (~1K/s) and thin (5 μm) filler metal was used. They also found that the likelihood of solidification at temperatures between the melting point of the filler alloy and the bonding temperature increased significantly when high diffusivity melting point depressant such as boron containing filler metal were used.

2.2 Modeling of TLP Bonding:

Much modeling research on *TLP bonding* process to date has involved the use of analytical methods [28,39,83] and treated the joining process as a number of discrete steps, namely, base metal dissolution, isothermal solidification and homogenization. Local equilibrium at the melting interface is generally assumed, as described before, when modeling two phase diffusion controlled problems. However, this is an approximation, since it is generally not attained at the solid/liquid interface [84]. Also, it is generally assumed that the formation of the liquid phase assures complete wetting of the base metal and production of a sound joint and this may not necessarily occur during *TLP Bonding*. For the sake of simplicity, it is assumed that the output of any stage does not affect the operating conditions that apply in the subsequent stages of the process.

2.2.1 Base Metal Dissolution:

The dissolution of base metal is inevitable during *TLP Bonding* [29]. Nakao *et al.* [52] and later on Nishimoto *et al.* [28] studied isothermal dissolution of base metal during TLP bonding based on the Nernst – Brunner theory [85]:

$$C = C_{sat}\left[1 - e^{-K(A/V)t}\right] \qquad (2.1)$$

where, C is the solute concentration in the liquid, C_{sat} is the saturated solute concentration, K is the dissolution rate, V is the volume of liquid, t is the holding time and A is the area of solid/liquid interface. They assumed that the total amount of solute in the

liquid remains constant and differentiated equation (2.1) to produce the following relationship for the dissolution parameter, P:

$$P = Kt = h\left[\ln\left\{\frac{X_s(X + ph)}{ph(X_s - X)}\right\}\right] \quad \ldots\ldots\ldots\ldots\ldots\ldots\ldots\ldots\ldots\ldots \text{(2.2)}$$

where, X is the width of the base metal dissolved at time t, X_s is the saturated dissolution width, p is the ratio of liquid density to solid density and h is half of initial liquid width. Nishimoto *et al.* [28] used equation (2.2) to compute the amount of base metal being dissolved (P) and showed that it varied linearly with holding time, as shown in Fig. 2.2(a), demonstrating that Nernst – Brunner theory could be used to explain dissolution of base metal during *TLP Bonding*. They also showed that the apparent activation energy for dissolution of base metal can be obtained using an Arrhenius plot, as shown in Fig. 2.2(b).

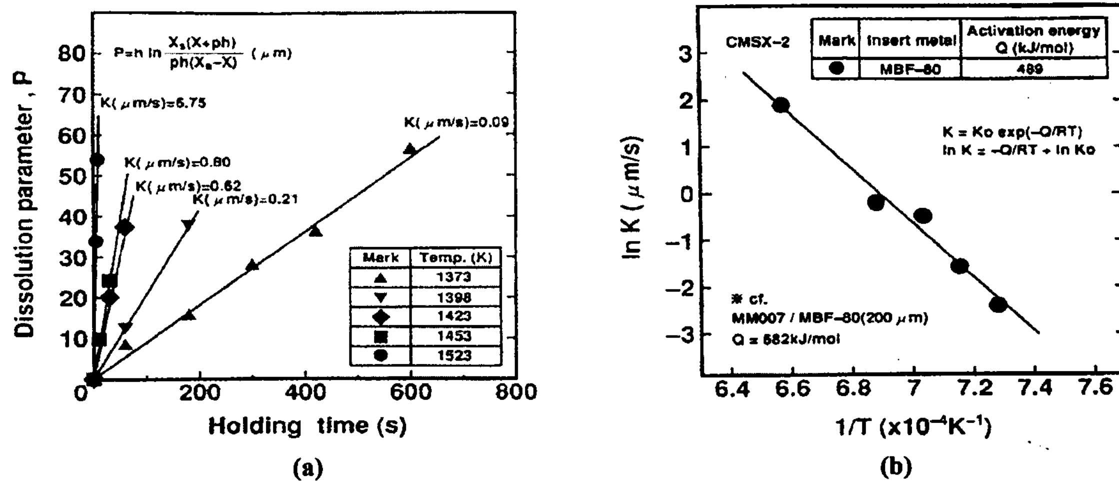

Fig. 2.2 Relation between (a) holding time and the dissolution parameter and (b) ln(K) and 1/T (CMSX-2/MBF-80 with an initial gap of 40 μm) [28]

Liu *et al.* [86] developed a model that accounts for base metal dissolution during liquid formation where they used a general error function solution to describe the solute distribution in the liquid zone when modeling the dissolution stage. However, they assumed that there is no solute diffusion into the base metal, which is not the case in actual practice, as solute diffusion can affect the process kinetics during the base alloy dissolution. On the other hand, Zhang and Shi [29] proposed a quantitative model for evaluating dissolution width which takes into account the process parameters, such as temperature, time and joint gap:

$$W_t = \left(\frac{\rho_L}{\rho_m}\right) C_L W_B \left[1 - e^{\left(-\frac{\alpha t}{W_B}\right)}\right] \quad \text{(2.3)}$$

where, W_t and W_B are the dissolution width and the initial joint gap, respectively, C_L and α are the solubility and dissolution coefficient, respectively, of the solid metal in the liquid metal (both are temperature and pressure dependent constants), ρ_L and ρ_m are the densities of the liquid metal and base metal, respectively.

It should be noted here that analytical methods developed so far are all based on assumptions that are very difficult to apply in modeling the dissolution of base alloys [43] and direct experimentation is required for the combination of base and filler alloys being used.

2.2.2 Modeling of Isothermal Solidification

The isothermal solidification stage is generally considered to be the most important stage since the time required for the entire *TLP Bonding* process is largely dependent on

the time required for completion of isothermal solidification. Several models have been proposed [7,46,83,87] to predict the isothermal solidification time during *TLP Bonding*. Solute distribution in the liquid can be considered to be uniform [43] during this stage. In addition, the base metal can be assumed to be semi-infinite since solute diffusion in the solid is generally slow. These models can be categorized according to the analytical descriptions used in the formulation of governing equations and are given below:

Stationary solid/liquid interface model:

The simplest modeling approach for predicting isothermal solidification time is the *stationary solid/liquid interface model*, alternatively known as *single phase solution model*. It treats the system as a single semi-infinite phase (the base metal) with a constant solute concentration ($C_{\alpha L}$) at the surface of the base metal, as shown in Fig. 2.3. The main advantage of this approach is that the final liquid width at the end of dissolution and liquid homogenization does not need to be calculated which requires extensive experimental investigations and/or complex model calculations to account for the moving boundary.

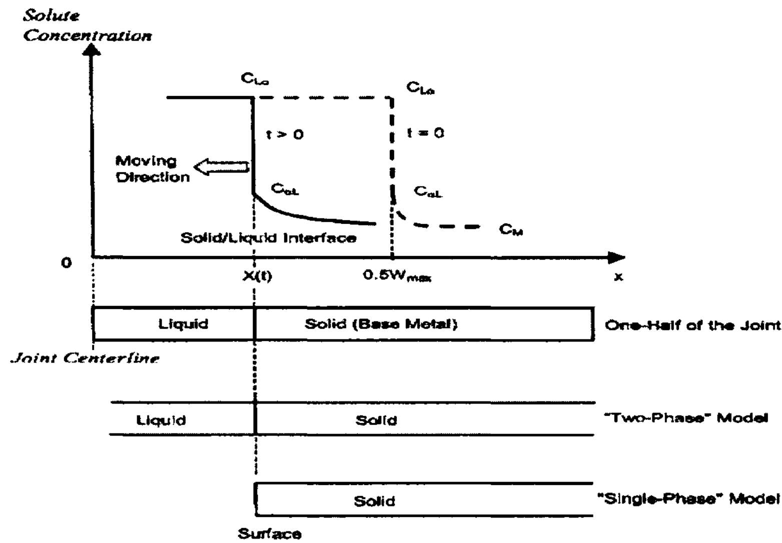

Fig. 2.3 Schematic diagram showing solute distribution during the isothermal solidification stage in *TLP Bonding* [88]

Tuah-Poku *et al.* [83] derived an expression for isothermal solidification completion time for silver/copper/silver sandwich joint based on stationary solid/liquid interface which can also be derived from the classical solutions for Fick's law. In order to describe the solute distribution in the semi-infinite base metal with a surface on which the solute concentration was maintained at $C_{\alpha L}$, an error function solution can be assumed [83,88]:

$$C(x,t) = C_{\alpha L} + (C_M - C_{\alpha L}) erf\left(\frac{x}{2\sqrt{(Dt)}}\right) \qquad (2.4)$$

where, $C_{(x,t)}$ = solute concentration as a function of distance from the centre of the interlayer (x) and time (t), $C_{\alpha L}$ is the solute concentration at the surface, C_M is the initial

solute concentration in the base alloy, D is the solute diffusivity in the base alloy. The total amount of solute M, which has entered into the base alloy at time t, can be determined using the following equation [88]:

$$M(t) = 2(C_{\alpha L} - C_M)\sqrt{\frac{Dt}{\pi}} \quad \text{..........(2.5)}$$

Ignoring the amount of solute diffused into the base alloy during the heating and dissolution stages, the total amount of solute diffused into the base alloy when the isothermal solidification is complete can be considered equal to the original solute content of the filler alloy excluding the amount which is dissolved in the solid solution, i.e.

$$C_F W_0 = 4(C_{\alpha L} - C_M)\sqrt{\frac{Dt}{\pi}} \quad \text{..........(2.6)}$$

where, C_F is the original solute concentration in the filler alloy and W_0 is the initial width of the filler alloy. Rearranging the above equation, the time required to complete isothermal solidification can be obtained as [83,88]:

$$t = \frac{\pi}{16D}\left(\frac{C_F W_0}{C_{\alpha L} - C_M}\right)^2 \quad \text{..........(2.7)}$$

Similar solutions were also derived by Ikawa *et al.* [46], Nakao *et al.* [89] and Onzawa *et al.* [61]. Tuah-Poku *et al.* [83] calculated the holding time required for silver/copper/silver sandwich joints based *on stationary solid/liquid interface* and their predicted values were found to be much higher than the experimentally determined values. They acknowledged the inadequacy of their mass conservation approach; however, they also attributed the discrepancy to the very complex conditions prevailing at the *moving solid/liquid interface*. Lee *et al.* [90] suggested that diffusion of the solute atoms into the base metal could actually take place during liquid homogenization, which could result in the formation of second phase precipitates and thus the holding time required for complete isothermal solidification would be considerably reduced.

Solute Distribution Model:

According to Crank [91], unsteady state diffusion of a specie from a source with initial thickness 2w, which is of the order of diffusion distance $\sqrt{(Dt)}$, into a semi-infinite substrate can be represented by:

$$C_{(x,t)} = C_M + \frac{1}{2}(C_0 - C_M)\left\{ erf\,\frac{x+w}{2\sqrt{Dt}} - erf\,\frac{x-w}{2\sqrt{Dt}} \right\} \qquad (2.8)$$

where, C_M = initial solute concentration in the base metal; C_o = initial solute concentration in the interlayer; $C_{(x,t)}$ = solute concentration as a function of distance from the centre of the interlayer (x) and time (t); D = diffusion coefficient of the solute in the substrate.

Holding time can be estimated considering the fact that isothermal solidification is completed when the solute concentration at the centre of the interlayer is reduced to the solidus value $C_{\alpha L}$. Substituting $C_{(x,t)} = C_{\alpha L}$ at $x = 0$ yields the following equation:

$$C_{\alpha L} - C_M = (C_0 - C_M)\left\{ erf \frac{w}{2\sqrt{Dt_f}} \right\} \qquad (2.9)$$

Several researchers [2,18,92] used this approach to predict the isothermal solidification time during *TLP Bonding* and to predict the precipitation of second phases in the substrate. They reported good agreement between estimated and experimental values. However, they used the linear relationships between the eutectic width and square root of holding time to get the extrapolated isothermal solidification time, e.g. Fig. 2.4, which suffers from the drawback that the time used in the model equation is not the actual one, and the complexity in measuring exact eutectic width poses a big challenge on the assumption of linear relationship between the eutectic width and square root of holding time.

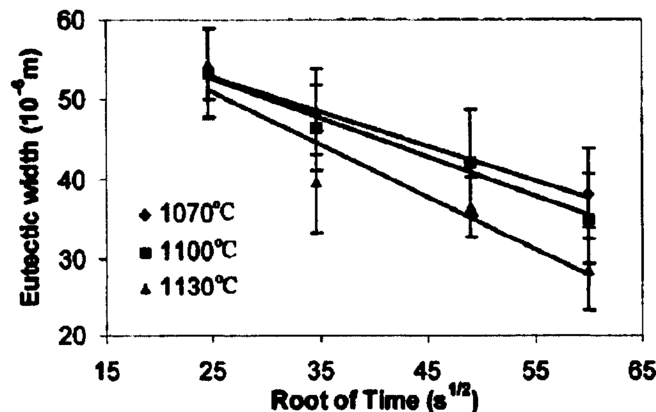

Fig. 2.4 Eutectic width vs. square root of holding time (Inconel 738/Nicrobraz 150 combination with an initial joint gap of 75 μm) [2]

Moreover, they used only two extrapolated isothermal solidification times to solve the diffusion equations in order to obtain the activation energy and frequency factor, which is not representative for real life *TLP Bonding* experiments that involve numerous physical and chemical uncertainties.

Migrating Solid/liquid Interface Model:

The diffusion controlled isothermal solidification stage of *TLP Bonding* consists of a process that involves a moving boundary. The *migrating solid/liquid interface model*, alternatively known as *two phase solution model*, treats the system as two semi-infinite phases with a coupled diffusion controlled moving solid/liquid interface, as shown in Fig. 2.3. A general error function solution, equation (2.10), can again be assumed to calculate the concentration of solute atoms in the solid phase [7,88,93,94].

$$C(x,t) = A_1 + A_2 erf\left(\frac{x}{2\sqrt{Dt}}\right) \quad (2.10)$$

where, $C_{(x,t)}$ = solute concentration as a function of distance from the centre of the interlayer (x) and time (t); A_1 and A_2 are constants that can be determined from the specific boundary conditions. When $x \longrightarrow \infty$

$$C(\infty,t) = A_1 + A_2 = C_M \quad (2.11)$$

At the moving solid/liquid interface, i.e., $x = X(t)$, solute concentration can be represented by:

$$C(X(t),t) = A_1 + A_2 erf\left(\frac{X(t)}{2\sqrt{Dt}}\right) = C_{\alpha L} \quad \text{.......................... (2.12)}$$

where $C_{\alpha L}$ is the solute concentration of the solid phase at the moving solid/liquid interface. If equation (2.12) is true for all values of t, $X(t)$ has to be proportional to $t^{1/2}$ as:

$$X(t) = 2\gamma\sqrt{Dt} \quad \text{.. (2.13)}$$

where γ is a constant that accounts for the moving boundary. The mass balance at the solid/liquid interface gives the following relation [7,88]:

$$(C_{L\alpha} - C_{\alpha L})\frac{dX(t)}{dt} = D\left(\frac{\partial C(x,t)}{\partial x}\right)_{x=X(t)} \quad \text{.......................... (2.14)}$$

where $C_{L\alpha}$ is the solute concentration of the liquid phase at the moving solid/liquid interface. The following relationship can be obtained by solving equations (2.10-2.14) [7,88,96] and is used to determine the parameter for moving boundary, γ:

$$\frac{C_{\alpha L} - C_M}{C_{L\alpha} - C_{\alpha L}} = \gamma\sqrt{\pi}\exp\gamma^2(1 + erf(\gamma)) \quad \text{.............................. (2.15)}$$

Now, from equation (2.13), the time required to complete isothermal solidification during *TLP Bonding* can be determined using the following relationship:

$$t_f = \frac{(2h)^2}{16\gamma^2 D} \quad \text{(2.16)}$$

where $2h$ is the final maximum width of the molten zone.

Several researchers, such as Ojo *et al.* [2], Sakamoto *et al.* [7], Ramirez and Liu [95], Zhou [96] etc., used the *migrating solid/liquid interface* approach, to predict the isothermal solidification time during transient liquid phase bonding because, unlike stationary solid/liquid model, it takes into consideration the moving boundary that exists during the isothermal solidification stage. However, Zhou [88] showed that equation (2.7) is a good approximation of equation (2.16) when C_M and $C_{\alpha L}$ are very small and $C_{L\alpha}$ is relatively large. A relatively small C_M and $C_{\alpha L}$ compared with $C_{L\alpha}$ will result into a very small value of γ, the parameter for the moving boundary, and hence a very slow solidification rate as evident from equation (2.13). Therefore, in such conditions, the migrating solid/liquid interface can be reasonably approximated by a stationary interface [88].

For $\gamma < 0.1$, a linear approximation exists between $t_f^{1/2}$ and $(2h/D^{1/2})$ [97], and Nakao *et al.* [87] developed the following linear expression:

$$t_f^{1/2} = J\left(\frac{2h}{D^{1/2}}\right) \quad \text{(2.17)}$$

where J is a dimensionless parameter and is related to γ by equation (2.16) through t_f. By their modeling of a moving solid/liquid interface, Nishimoto *et al.* [28] showed that for multi-component migrating solid/liquid interface conditions, the following relationship exists:

$$\ln(m) = A - \frac{Q}{2RT} \quad \text{.. (2.18)}$$

where m is the slope of the plot of the eutectic width against the square root of holding time, Q is the apparent activation energy for diffusion of melting point depressant into the base metal, T is the absolute bonding temperature, R is the gas constant and A is a constant. If the frequency factor (D_0) is known, diffusion coefficient of melting point depressant at any bonding temperature can be determined using the obtained activation energy (Q) and the following an Arrhenius relationship:

$$D = D_0 e^{(-\frac{Q}{RT})} \quad \text{.. (2.19)}$$

Equation (2.17) can then be used to predict the time requirement to complete isothermal solidification. However, in order to use equation (2.17), J has to be determined using $t_f^{1/2}$ vs. $(2h/D^{1/2})$ plot, e.g. Fig. 2.5.

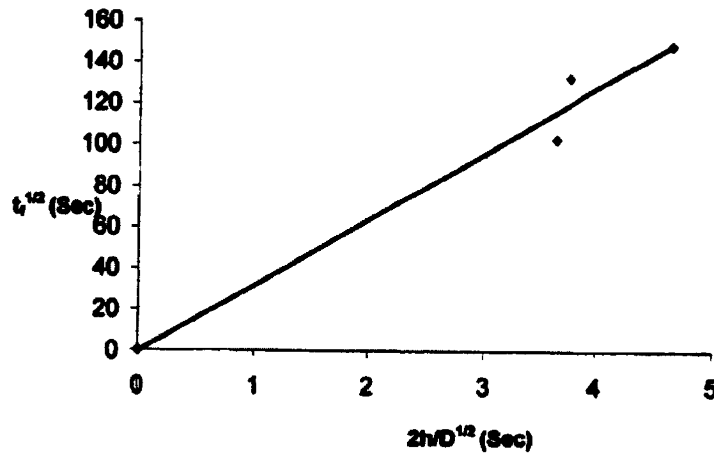

Fig. 2.5 $t_f^{1/2}$ vs. $(2h/D^{1/2})$ plot to determine J of equation (2.17) [26]

Since this method relies on the linear relationship between eutectic width and square root of holding time, it suffers from the same drawbacks as mentioned earlier. Also, linear relationship between $t_f^{1/2}$ and $(2h/D^{1/2}$ is only an approximation and used to avoid complex numerical calculation of γ and its variation with temperature. Moreover, when the frequency factor (D_0) for diffusion of melting point depressant is not known, calculation of γ cannot be avoided.

It should be noted here that, although *migrating solid/liquid interface* modeling approach was used by several researchers, none of them took into consideration the physical and chemical uncertainties associated with the *TLP Bonding* experiments. All of them reported one single set of kinetic parameters, such as activation energy and frequency factor, for each of the combination of base and filler metals which has very limited practical value.

2.2.3 Homogenization Stage:

Ikawa *et al.* [46] used equation (2.20) to model the solute distribution during homogenization of *TLP Bonding* with nickel based superalloy material.

$$C_{(x,t)} = C_M + \frac{1}{2}(C_0 - C_M)\left\{ erf\,\frac{x+w}{2\sqrt{Dt}} - erf\,\frac{x-w}{2\sqrt{Dt}} \right\} \text{........(2.20)}$$

where w was half the maximum liquid width at the end of base metal dissolution and C_0 was equal to C_{La}. The solute concentration attained its maximum value at the centerline of the specimen ($x=0$) which can be represented by [53]:

$$C_{max} = C(0,t) = C_M + (C_0 - C_M)erf\left[\frac{w}{2\sqrt{D_s t}}\right] \text{.......................... (2.21)}$$

Nakao *et al.* [53] observed good agreement between the results predicted by equation (2.21) and the experimentally determined values for most of the homogenization period of nickel base superalloy material although a distinct difference between the analytical calculations and the experimental values during the early stages of the homogenization treatment was observed. According to Nakao *et al.* [53], this difference was due to the critical assumption in the analytical results that the aluminum concentration in the joint centerline was uniform at the beginning of the homogenization period. Zhou [96] also used equation (2.21) to model the homogenization stage during *TLP Bonding*. In his study, w was taken as half the filler alloy thickness and C_0 the initial solute concentration. Since the final liquid width need not be calculated, which requires extensive experimental investigations, this method is quite simple and easy to use [43].

Chapter 3

Scopes of Present Investigations

Several researchers used different mathematical modeling approaches, as mentioned in section 2.2.2, to predict the isothermal solidification time during *TLP Bonding* of pure nickel, nickel based single crystal superalloys, precipitation hardened nickel based polycrystalline superalloy such as Inconel 738, and also for duplex stainless steel base metals with binary Ni-P or ternary Ni-Cr-B, or multi-component Ni-B-Cr-Si-Fe filler alloys, and reasonable agreement with the experimental values have been reported. However, modeling studies and experimental investigations of isothermal solidification during TLP bonding of Inconel 625 and 718 superalloys, and SS 410 and SS 321 with a multicomponent filler alloy, BNi-2, could not be found in the literature.

Mathematical modeling coupled with experimental data is widely used to determine the kinetic parameters such as diffusion coefficient of solute atoms into the base alloys during transient liquid phase bonding. However, when coupling experimental data with the mathematical model, the physical and chemical uncertainties associated with the diffusion brazing experiments needs to be addressed in a way that it best reflects the diffusion characteristics of the solute atoms into the base alloy. Taking only one or two sets of experimental data, often sufficient to solve the governing diffusion equations, will lead to erroneous results because another set of experimental data will result in a different value. Also, in conventional modeling technique, these one or two sets of

experimental isothermal solidification times are usually taken from the eutectic widths versus square root of holding time diagrams where a linear relationship is assumed i.e. when the eutectic widths are extrapolated to zero value, the corresponding holding time will represent the isothermal solidification time. This is the biggest source of error because of the extreme difficulty in measuring eutectic widths and also the use of extrapolated values instead of real values. However, the errors could not be avoided in previous studies because the use of constant gap joints does not allow determining the exact isothermal solidification time.

The problem of getting real experimental isothermal solidification times can be eliminated if V-shaped joints are used to determine the maximum brazing clearances. The details will be described later in Chapter 4 and 5. In order to take into consideration the physical and chemical uncertainties associated with *TLP Bonding* experiments, several sets of real experimental data need to be used to determine the range of diffusion coefficients and it can be then modeled as a random number based on the statistical distribution profile being observed, such as normal, weibull or any other distribution. Such modeling approach is known as Random Walk Modeling and is widely used to simulate the diffusion characteristics of solute atoms in diffusion governing processes [98-103]. However, this approach has not been used so far to simulate the diffusion characteristics of solute atoms into the base alloys during *TLP Bonding* and, single sets of kinetic parameters for diffusion of solute atoms continue to appear in literature which is not representative for real life experiments.

Hence, the objectives of this work are to calculate the time required to complete isothermal solidification during transient liquid phase bonding of Inconel 718 and 625

superalloys, and SS 410 and 321 with BNi-2 filler alloy using mathematical models based on migrating solid/liquid interface and solute distribution law taking the random diffusion of solute atoms into considerations, and to verify the predicted isothermal solidification times with experimental investigations.

Diffusion models for *TLP Bonding* with nickel based filler alloys containing boron as the major melting point depressant rely on the solubility limit of boron in pure nickel as a reference to form solid solution. This assumption is reasonable when pure nickel or nickel based superalloys are used as base metals. However, when stainless steels are used as base metals, such as SS 410 and SS 321, significant amount of iron comes into the melt due to the dissolution of the base metal. It is, therefore, also an objective of this study to verify this assumption when martensitic stainless steel, SS 410, with almost negligible amount of nickel in its composition, and austenitic stainless steel, SS 321, with significant amount of nickel and chromium in its composition, are used as base alloys. Besides, the use of silicon, which also acts as a melting point depressant, as a reference element to form solid solution will be verified.

Chapter 4

Experimental Procedures

4.1 Materials:

The brazing filler metal selected for this research is BNi-2 (AMS 4777) which is a nickel based multi-component filler alloy with boron and silicon as melting point depressants. Four different wrought base alloys were chosen that are extensively used in aero-engine hot section components and in many other applications that require excellent strength and ductility at elevated temperature. Two of them are austenitic nickel based polycrystalline superalloys, Inconel 625 and Inconel 718, and the remaining two were martensitic stainless steel, SS 410, and austenitic stainless steel stabilized with titanium, SS 321. The nominal compositions of the base and filler alloys along with their melting temperatures are given in Table 4.1.

4.2 Wedge-Gap Specimens and Brazing Procedures:

Wedge shape joint gap specimens with identical base alloys, shown in Figure 4.1, were utilized to form an edge groove where the BNi-2 brazing filler paste was placed. The specimen was fixed by tack welds to form a variable brazing gap (0 – 250 μm). The wedge gap specimens have the advantage over the constant width joints that it provides variable joint gap widths which can be tested at the same temperature and time. Since the initial V-configuration is known, the dissolution of the base metal can be determined at

any location of interest within the specimen using the similarity principle of triangles and subsequently, the maximum brazing clearances for different process conditions can be obtained.

Table 4.1 Nominal compositions of Inconel 625, Inconel 718, SS 410, SS 321 and BNi-2

Alloy	Nominal Composition (wt%)	Solidus (°C)	Liquidus (°C)
Inconel 625	Ni: 58% (min), Cr: 20 – 23%, Fe: 5%, Co: 1%, Mo: 8 – 10%, Nb(+Ta): 3.15 - 4.15%, Ti: 0.4%, Al: 0.4%, C: 0.1%, Mn: 0.5%, Si: 0.5%	1290	1350
Inconel 718	Ni (+Co): 50-55%, Cr: 17-21%, Fe: bal, Co: 1%, Mo: 2.8-3.3%, Nb(+Ta): 4.75-5.5%, Ti: 0.65-1.15%, Al: 2-8%, C: 0.8%, Mn: 0.35%, Si: 0.35%, B: 0.006%, Cu: 0.3%	1260	1336
AISI 410	Fe, <0.15%C, 11.5-13.5%Cr, >0.75%Ni, <1.0%Si, <0.04%P, <0.03%S	1480	1530
AISI 321	Fe, <0.08%C, 17-19%Cr, 9.0-12.0%Ni, <0.75%Si, <0.045%P, <0.03%S, <0.7% Ti [5*(N+C) min], <0.1%N, <2.0%Mn	1371	1399
BNi-2	Ni-7Cr-3.2B-4.5Si-3Fe-0.06Cmax	971	999

The samples were nicro-blasted and then acid cleaned. To prevent the oxide build-up, the base alloy was pre-plated with very thin layer (≈ 5 μm) of nickel (nickel flash). A vacuum inert gas atmosphere furnace was used for brazing where the chamber pressure could be set at 1.33 mPa (10^{-5} torr) to 106.6 Pa by controlling the flow rate of highly purified argon into the chamber. To study the effect of major process variables, such as temperature, holding time and joint gap, on the time required to complete

isothermal solidifications, the samples were brazed according to the matrix shown in Table 4.2. Two replicas were taken for each of the process conditions to ensure the repeatability.

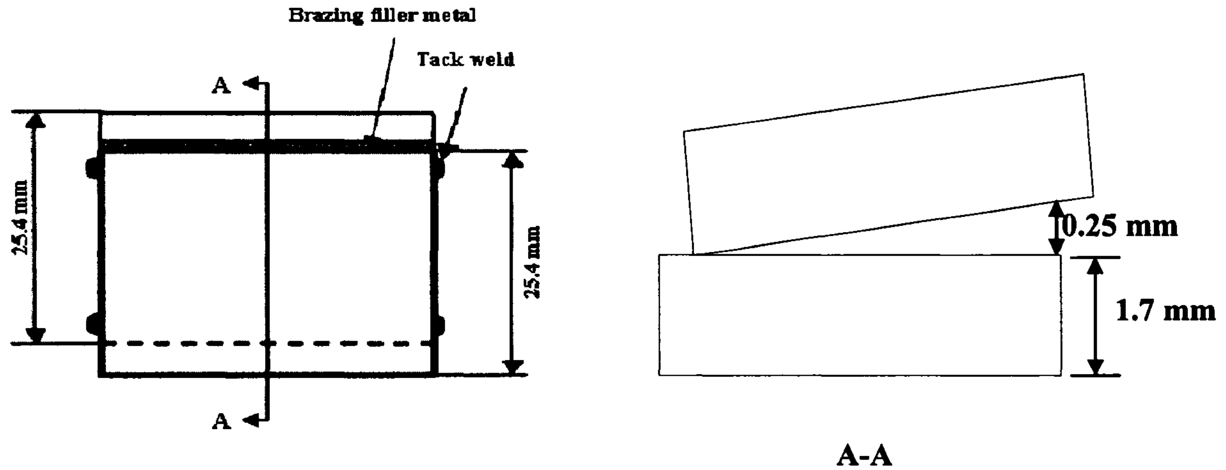

Fig. 4.1 The wedge shape joint gap specimen

Table 4.2 Braze tests matrix

Temp. (K)	Holding Time (min)						
1325	10			50	60	70	90
1358			30	50		70	90
1394	10	20	30	50			90

All of the brazed joint samples were cut as per section A-A in Fig. 4.1, prepared metallographically using standard techniques and studied under the Olympus optical microscope equipped with Discover Essential Image Analyzer to measure the maximum brazing clearances and scanning electron microscope (SEM) equipped with electron dispersive spectrometry (EDS) to identify the different phases in the final brazed joint microstructures.

Chapter 5

Microstructures of the Joints and Related Measurements

5.1 Microstructures of Brazed Joint:

In metallographic terms, a good joint can be defined as one with similar properties of the base metals. However, previous investigations have shown that the microstructures developed in the joints brazed with nickel based filler alloys are rather complicated and, therefore, a better understanding of the solidification phenomena and formation of intermetallic compounds in these braze joints is the key to control and engineer the microstructures which have minimal weaknesses arising from the formation of brittle intermetallic compounds [6].

A typical metallographic microstructure of a brazing joint, when isothermal solidification is not completed, can be divided into three distinct zones, namely, the affected base metal area (zone I), the solid solution area (zone II) and the centerline eutectic area (zone III) [6,34], as shown in Fig. 5.1.

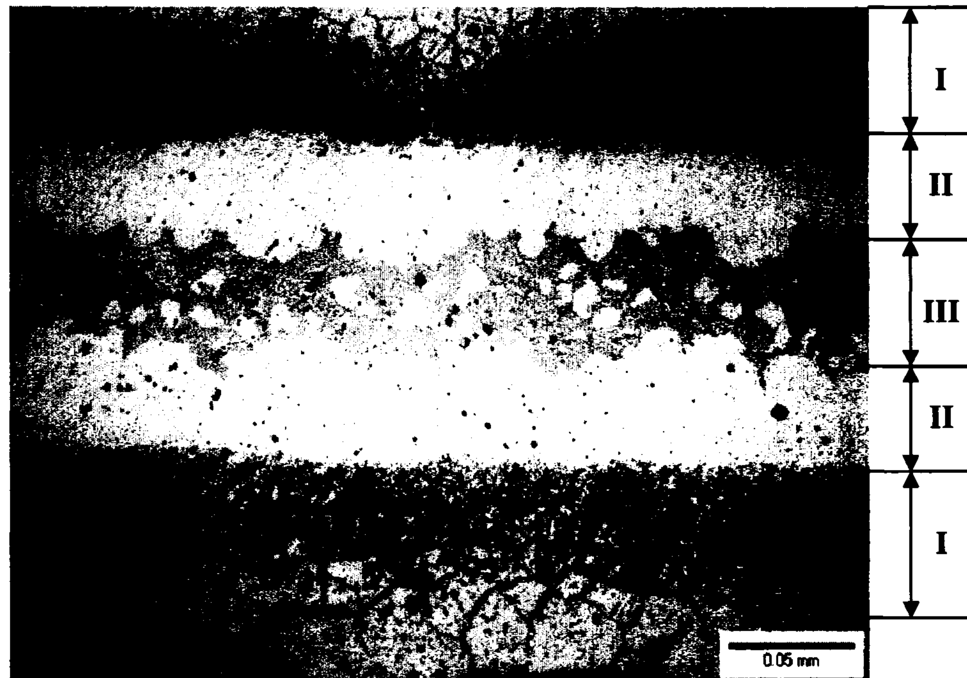

Fig. 5.1 Typical microstructure of a brazed joint showing three distinct areas (I: affected base metal, II: solid solution and III: centerline eutectics)

Zone I is the parent metal close to the gap where transgranular and intergranular precipitates are found [6,21,31,71]. The intergranular precipitates are found to be much deeper in the parent metal due to the rapid diffusion of melting point depressant along the grain boundaries. Because of that and its low solubility in the parent metal, precipitations take place with a very dense arrangement which in turn produce hardening of the parent metal and increase the brittleness of the area [14,17,71].

Zone II is the solid solution layer. It is formed isothermally at the brazing temperature [6,34].

Zone III is the eutectic area that forms during cooling down of the residual liquid when the holding time is not long enough to complete isothermal solidification [30]. This

area is of great concern because the melting point depressants form hard and very brittle intermetallic compounds which are detrimental to the mechanical properties of the joints.

5.1.1 Inconel 718/BNi-2 and Inconel 625/BNi-2:

The optical micrographs of Inconel 718/BNi-2 joint, with an initial joint gap of ≈ 70 μm, brazed at 1394K are shown in Fig. 5.2 to illustrate the effect of holding time on the formation of isothermally solidified joints. Since diffusion is a time dependent process and isothermal solidification is dependent on the diffusion of melting point depressants, the holding time plays the key role in obtaining the eutectic free joints. As expected, it was observed that the amount of brittle eutectic phases decreased with increasing brazing time.

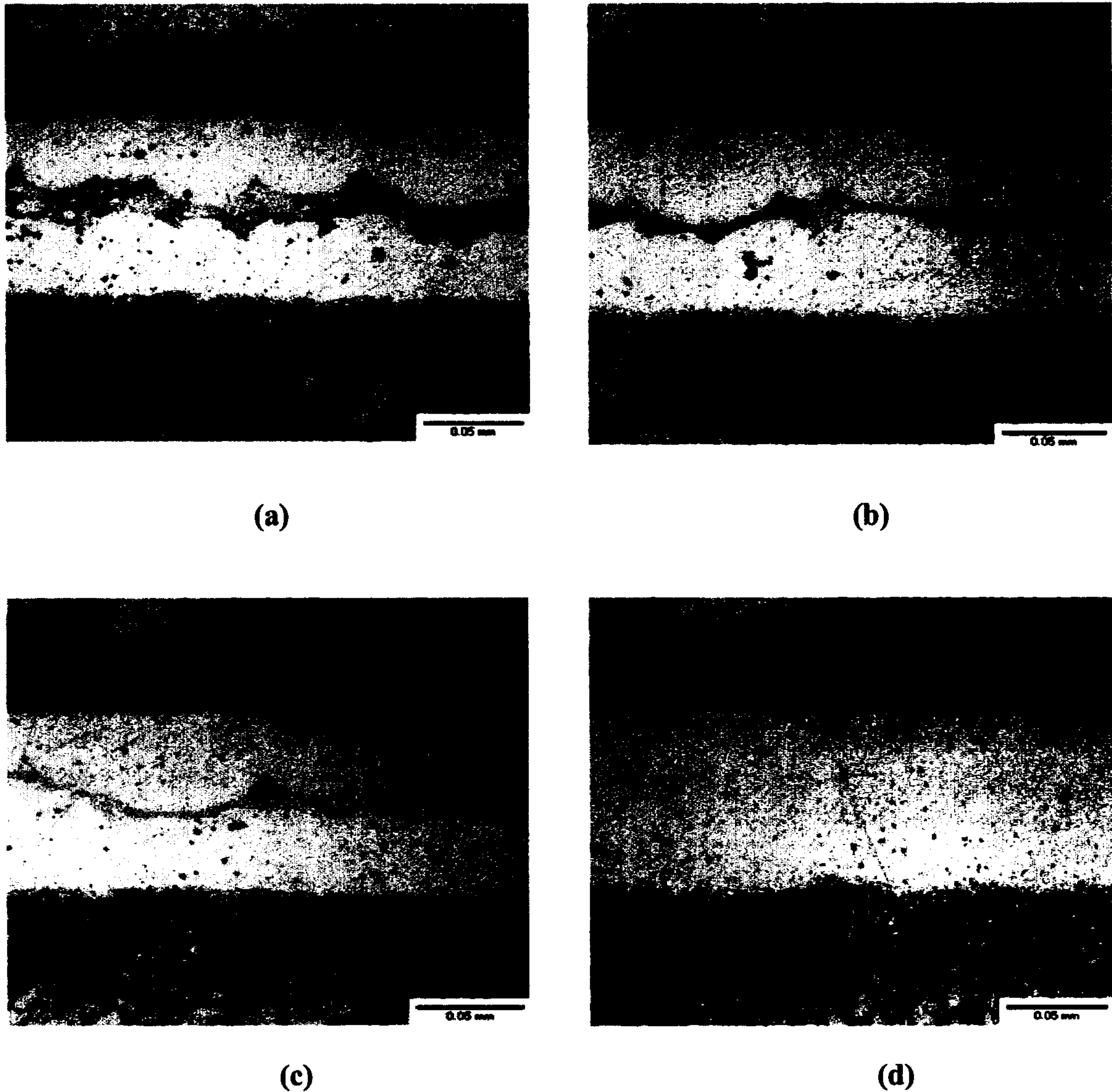

Fig. 5.2 Microstructures of the Inconel 718/BNi-2 joint, with an initial joint gap of ≈ 70 μm, brazed at 1394K for various lengths of times: (a) 10 min, (b) 20 min, (c) 30 min and (d) 50 min

Figure 5.2 (a) shows that large amount of eutectic phases remained in the centerline of the bond after holding for 10 minutes at the TLP brazing temperature. When the brazing time was prolonged to 20 minutes, the amount of brittle phase continued to

decrease. After 30 minutes of holding period, there still exist some eutectics. Further increase of holding time to 50 minutes resulted in complete isothermal solidification.

It was observed that initial joint gap thickness plays a significant role in the time requirement to complete isothermal solidification as shown in Fig. 5.3. This is because the wider the joint gap the higher the amount of boron which will take more time to diffuse out into the base metal.

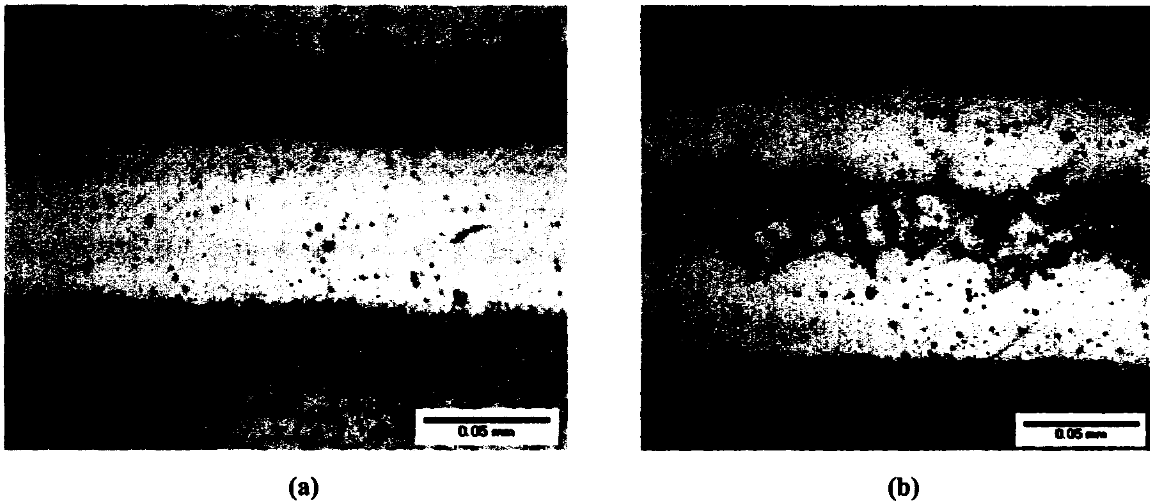

Fig. 5.3 Microstructures of Inconel 718/BNi-2 joints brazed at 1325K for 70 minutes with initial joint gaps of (a) ≈ 60 μm and (b) ≈ 100 μm

Figure 5.4 shows the effect of bonding temperature on the time required to complete isothermal solidification. Diffusivity increases with increasing temperature and, therefore, although the joint with an initial joint gap width of ≈ 70 μm solidified isothermally at 1394K after 30 minutes of holding time, isothermal solidification was yet to complete at 1358K bonding temperature for the same length of time. The width of the final brazed joint in Fig. 5.4 (b) was found to be slightly larger than that of Fig. 5.4 (a)

although the initial joint gap widths were same. This can be attributed to the fact that dissolution of base metal is higher at higher bonding temperature [28].

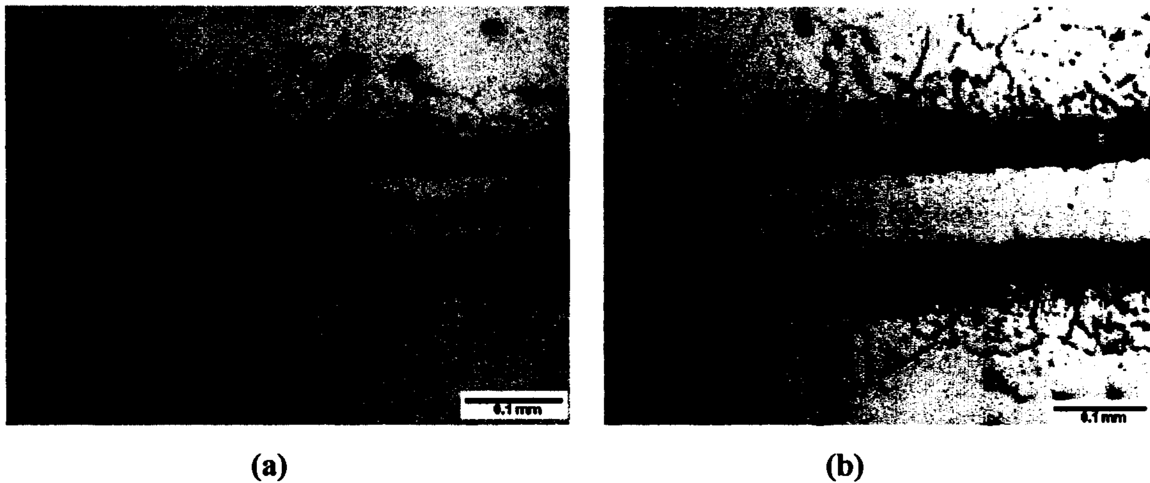

(a) (b)

Fig. 5.4 Microstructures of Inconel 625/BNi-2 joints brazed for 30 minutes at (a) 1358K and (b) 1394K

Phase Identifications:

A typical micrograph of the Inconel 625/BNi-2 brazed joint and the corresponding EDS analyses are shown in Fig. 5.5. Intermetallic phases were formed in the eutectic region. EDS analyses confirm that the phase marked *X1* is the pro-eutectic *γ-nickel* solid solution and the phases marked with *X2* and *X3* are *Cr* and *Ni* rich borides, which were also reported by other researchers [2,6,27,30]. EDS analyses of Fig. 5.5 detected significant amount of chromium in the precipitates in the interfacial areas compared to that in the surrounding *γ-nickel* matrix which suggest that they are mainly chromium rich borides.

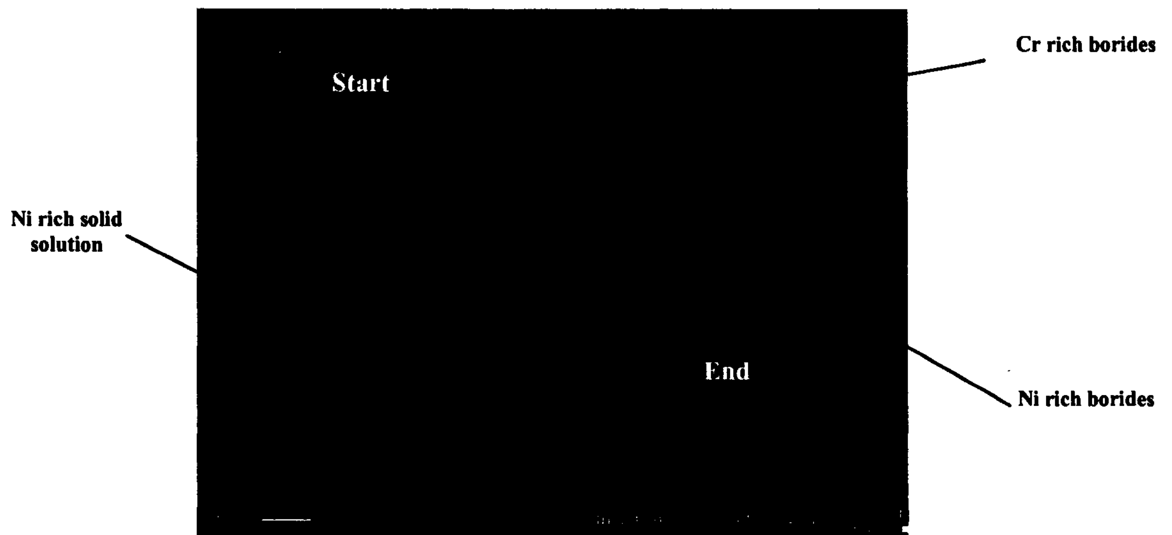

(a)

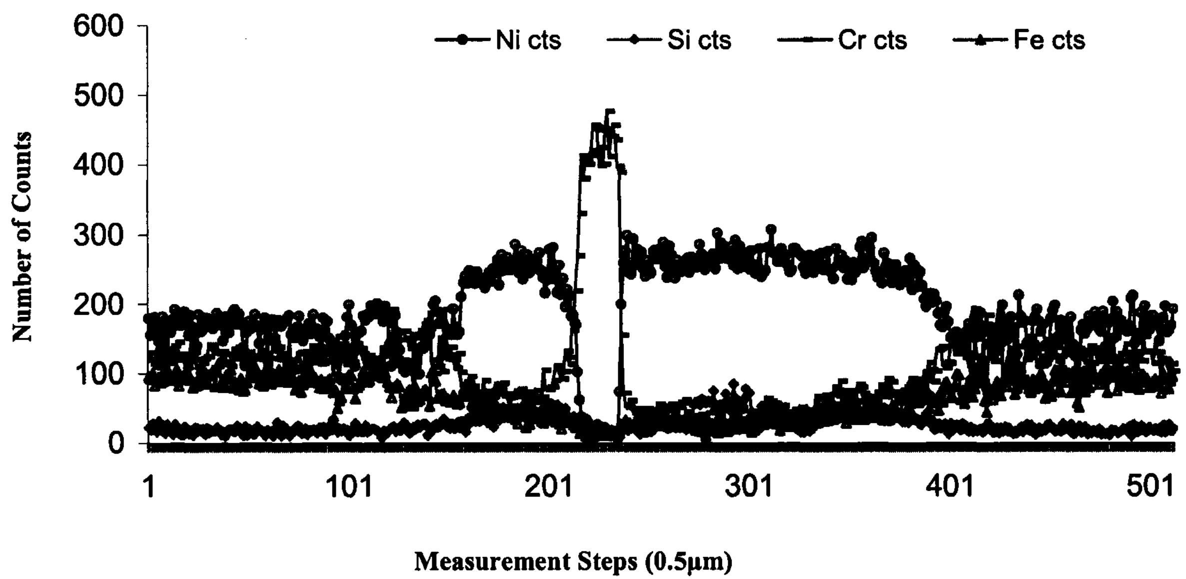

(b)

Fig. 5.5 (a) SEM micrograph of Inconel 625/BNi-2 joint brazed at 1325K for 10 minutes showing centerline eutectics, (b) EDS number of counts versus the measurement step (0.5 μm)

A magnified view of the centerline eutectic structures of Inconel 625/BNi-2 joint, as shown in Fig. 5.6, suggests that the microstructures evolved in nickel superalloy brazed joints are extremely complicated. This is due to the presence of several alloying elements in the base metal that come into the melt due to the dissolution. In a study of evaluation of transient liquid phase bonding between Inconel 718 and Inconel X-750 with BNi-2, Wu *et al.* [30] reported that niobium had appeared in the brazed center due to the dissolution of Inconel 718, and the degree of niobium at immediately adjacent to the bond was found to be relatively higher than that in Inconel 718 base metal because niobium carbides segregatged in the vicinity of liquid/Inconel 718 interface due to boron diffusion. They also detected titanium and molybdenum in the braze, and carbide precipitates in Inconel 718, in the vicinity of joint interface. Appearance of titanium and molybdenum was attributed to the dissolution of base metal and affinity of molybdenum to boron and silicon, and carbide precipitates to boron segregation because they were found only in the areas where there were boron segregations. Segregation of boron along the grain boundaries of base metals has one or more of the following effects: (i) increase grain boundary cohesion, (ii) reduction in grain boundary surface energy, (iii) lower grain boundary diffusion rates, and (iv) changes in γ' *($Ni_3(Al, Ti)$ cuboidal phase)* and/or $M_{23}C_6$ morphologies [30]. In the current study, the grain size adjacent to the joint interface was found to be much smaller than that far away from the interfacial area which was also the case in several previous *TLP Bonding* studies [2,7,30,34]. This can be attributed to the fact that boron induced carbide precipitation provides the pinning effect which retards the grain growth [30].

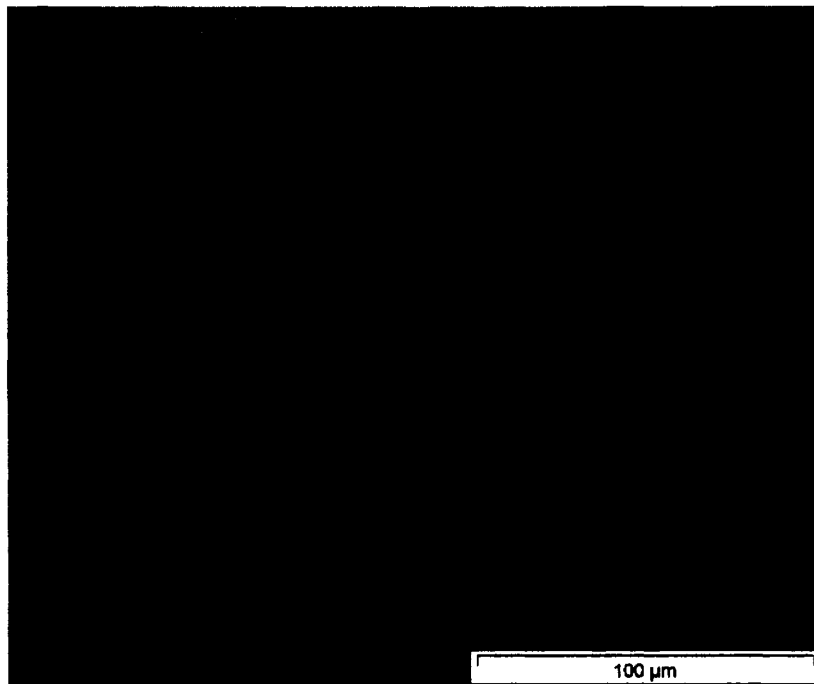

Fig. 5.6 Optical micrograph of Inconel 625/BNi-2 joint showing the centerline eutectic morphology

From the *Ni-Si* phase diagram [104], it is evident that *Ni* dissolves an average of 15 mol% Si over the brazing temperature range (1325K to 1394K), and thus it is expected to have little or almost no silicides. However, EDS compositional analyses in Fig. 5.5 (b) revealed a significant amount of silicon in the center of the joint that might form nickel silicides. This can be understood from the following solidification phenomenon [6]: During brazing, *γ-nickel* first solidified isothermally from the faying surfaces into the melt. Upon cooling the primary *γ-nickel* solidified as nodular dendrites which enriched the remaining melt with boron, silicon and chromium. As cooling proceeded, binary eutectic of *γ-nickel* and *nickel boride* occurred, further enriching the melt of *chromium.*

Subsequently, binary eutectic of *γ-nickel* and *chromium boride* solidified. The melt, which was further enriched in silicon, was then transformed into the ternary eutectic of *γ-nickel, nickel boride* and *nickel silicides*. Similar solidification phenomena are expected for the Inconel 625 and 718 superalloys with BNi-2 filler alloy when the holding times are not long enough to complete isothermal solidification.

5.1.2 SS 410/BNi-2 and SS 321/BNi-2:

SEM micrographs of the SS 410/BNi-2 brazed joint are shown in Fig. 5.7 and 5.8, and optical micrographs of SS 321/BNi-2 brazed joints are shown in Fig, 5.9. Like nickel superalloys, intermetallic phases were formed along the centerline of the joint as the samples were cooled before the isothermal solidification finished. However, the microstructures of both stainless steel base alloy, SS 410 and SS 321, joints are found to be less complicated than the superalloys since there are not as many alloying elements as there are in the nickel superalloys.

EDS analyses of Fig. 5.8 (a) show that the phase marked *X1* is the pro-eutectic *γ-nickel* solid solution and the phases marked with *X2* and *X3* are *Cr* and *Ni* rich borides. A line scan through the centerline eutectics of SS 410/BNi-2 joint, shown in Fig. 5.10, revealed significant amount of silicon in the centerline of the joint which might form nickel silicides. These are in agreement with the findings of Shiue *et al.* [31] who worked with martensitic stainless steel, SS 403, with BNi-2 filler alloy. EDS analyses of Fig. 5.7, 5.8 and 5.10 also revealed that iron concentration in the joint centerline had reached 14 wt% and 8 wt%, respectively, for SS 410/BNi-2 joints brazed at 1394K and 1325K for 50 minutes. The initial iron concentration in the BNi-2 filler alloy is 3 wt%, therefore, it is

obvious that significant amount of iron has diffused out into the braze joint from the base metal during the brazing process due to the dissolution of base metal and the amount of iron increased with increasing brazing temperature because dissolution thickness increases with increasing bonding temperature.

Extensive intergranular and transgranular precipitates were also observed at the interface between the base metal and the brazement, as shown in Fig. 5.7, 5.8 and 5.10. EDS analyses suggest that they are mainly chromium and iron rich borides. Shiue *et al.* [31] reported the same observation while studying the interface microstructures of SS 403 and BNi-2. According to their EPMA analyses, these phases are primarily comprised of *B*, *Cr* and *Fe*. The composition of SS 403 and SS 410 is very close to each other and similar conclusions can be drawn. Although the ternary *B-Cr-Fe* phase diagram is not entirely known, six ternary phases, *BCrFe*, $B_{33}Cr_{13}Fe_{54}$, $B_{33}Cr_{33}Fe_{34}$, $B_{38}Cr_{55}Fe_{7}$, $B_{50}Cr_{20}Fe_{30}$ and $B_{50}Cr_{35}Fe_{15}$ have been found in the diagram [105]. Therefore, formation of such phases is not unexpected; however, the exact stoichiometries of these phases were not confirmed by Shiue *et al.* [31] because the size of the ternary *B-Cr-Fe* phases were less than 1 μm which was smaller than the spot size being used in their EPMA analyses.

No EDS analyses of SS 321/BNi-2 brazed joints were carried out in this study, however, similar isothermal solidification phenomenon applies for this combination as well, that is the joint area is comprised of *γ-nickel* solid solution and when the holding time is not long enough the residual liquid will transform into *nickel* and *chromium* rich *borides* and *nickel silicides*. The morphologies of the centerline eutectic phases are very similar to the ones presented by Jang *et al.* [34] who worked with austenitic stainless steel, SS 304 with BNi-2 filler alloy and reported the abovementioned phases. The

composition of SS 304 is very similar to that of SS 321 except that there is no titanium in SS 304. Therefore, similar conclusions can be inferred. However, in addition to the intergranular and transgranular precipitates of chromium and iron rich borides, some globular precipitates were also observed in the interfacial area of the SS 321/BNi-2 joint, as shown in Fig. 5.9, because of the presence of Ti in the composition of SS 321 base alloy which acts as a stabilizing element. Zorc and Kosec [17] also reported this kind of precipitate while studying the high temperature SS 321/BNi-7 brazed joint microstructures. The fundamental reason to add *Ti* in SS 321 is to avoid intergranular corrosion. During welding or high temperature brazing, when steel goes through the sensitization stage (i.e. intergranular attack can occur) *titanium carbides* would form in preference to *chromium carbides* [106]. In doing so, *chromium* would remain in solution that produces the passive film of *chromium oxide* which makes the steel corrosion resistant. Similarly, titanium has a strong affinity to boron compared to *chromium* and when boron diffuses out towards the base metal, *titanium borides* (globular precipitates in the interfacial area of the joint) form in preference to the *chromium borides* [107]. However, the composition of *chromium* is much higher than that of *titanium* and, therefore, significant amount of intergranular *chromium boride* precipitates were also observed in the interfacial area of the SS 321/BNi-2 joint.

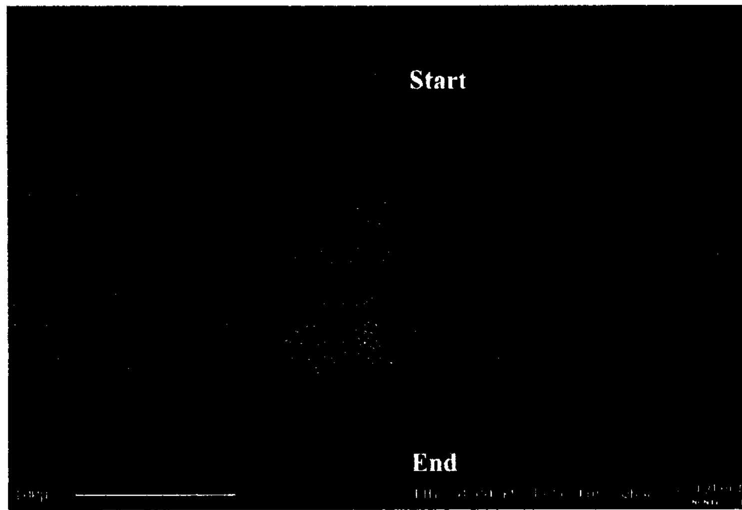

(a)

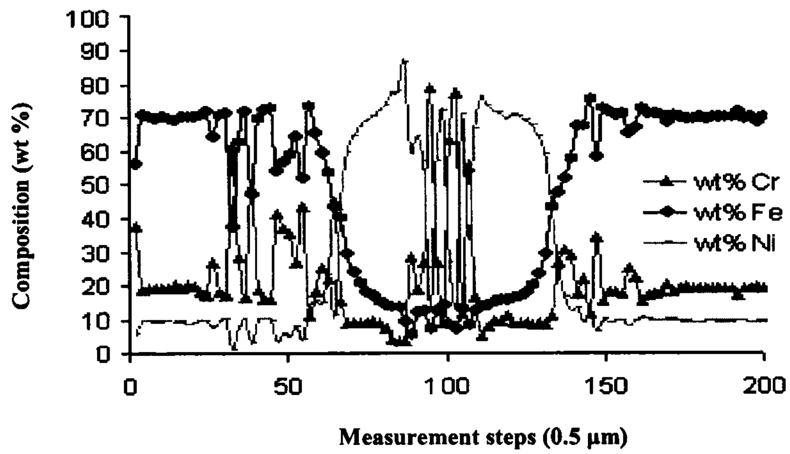

(b)

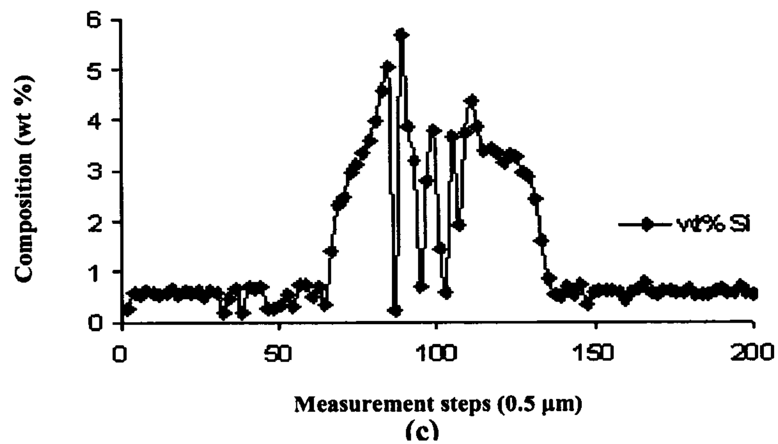

(c)

Fig. 5.7 (a) SEM micrograph of SS 410/BNi-2 joint brazed at 1394K for 50 minutes showing centerline eutectics, (b) and (c) EDS analyses

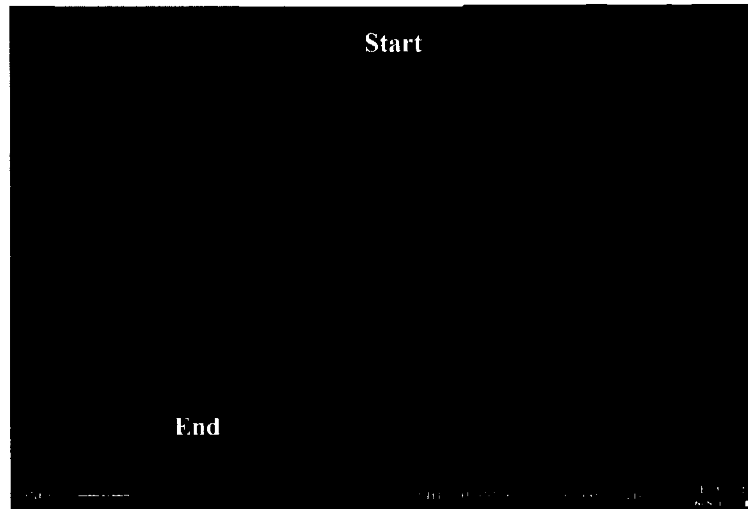

(a)

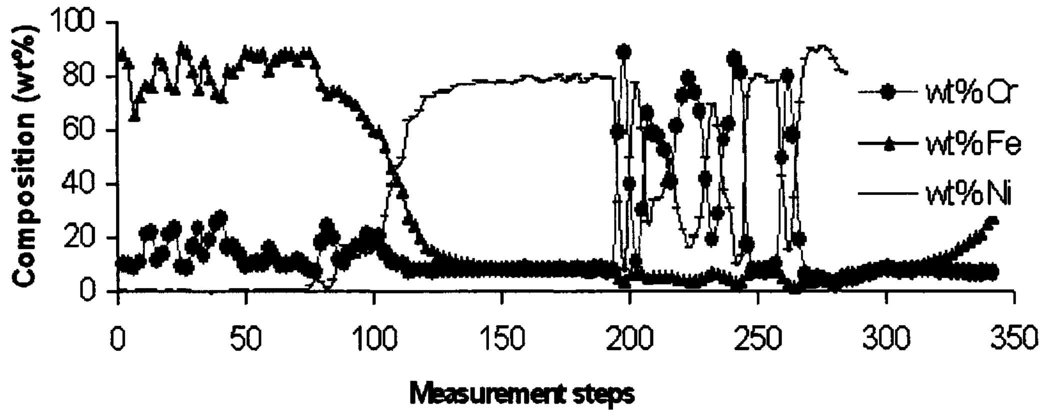

(b)

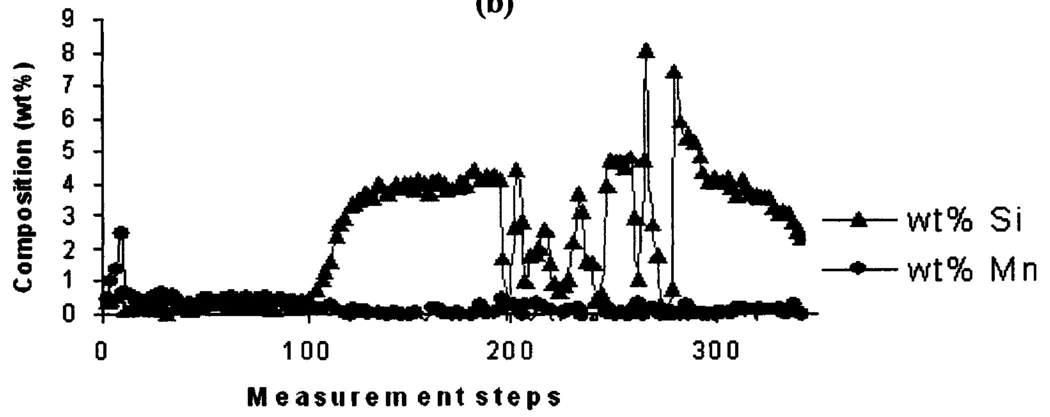

(c)

Fig. 5.8 (a) SEM micrograph of SS 410/BNi-2 joint brazed at 1325K for 50 minutes showing centerline eutectics, (b) and (c) EDS analyses

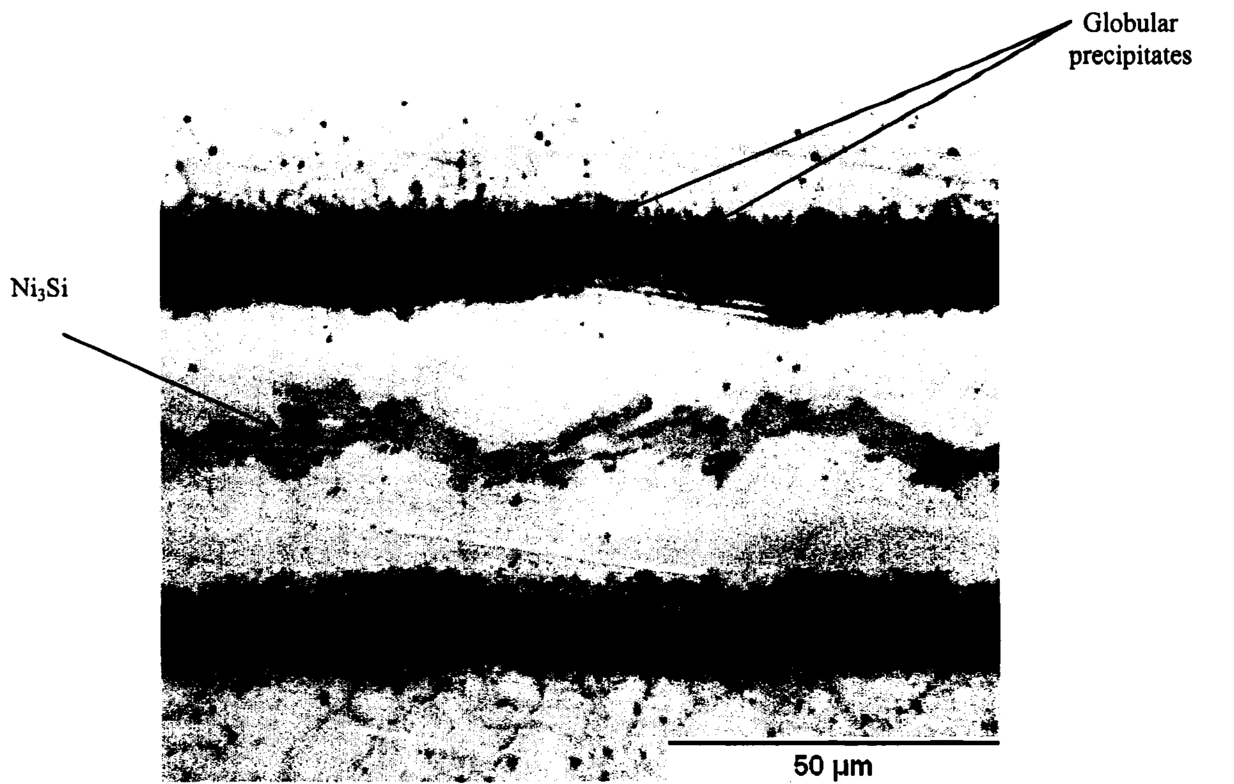

(a)

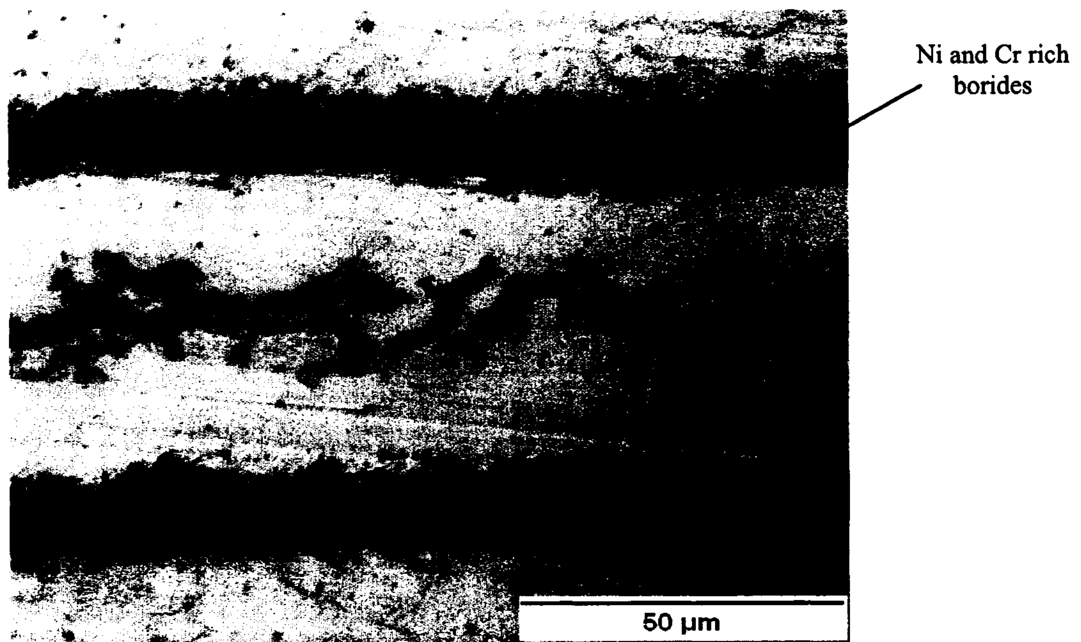

(b)

Fig. 5.9 Microstructure of a SS 321/BNi-2 joint brazed at (a) 1394K and (b) 1325K, for 10 minutes showing centerline eutectics and interfacial precipitates

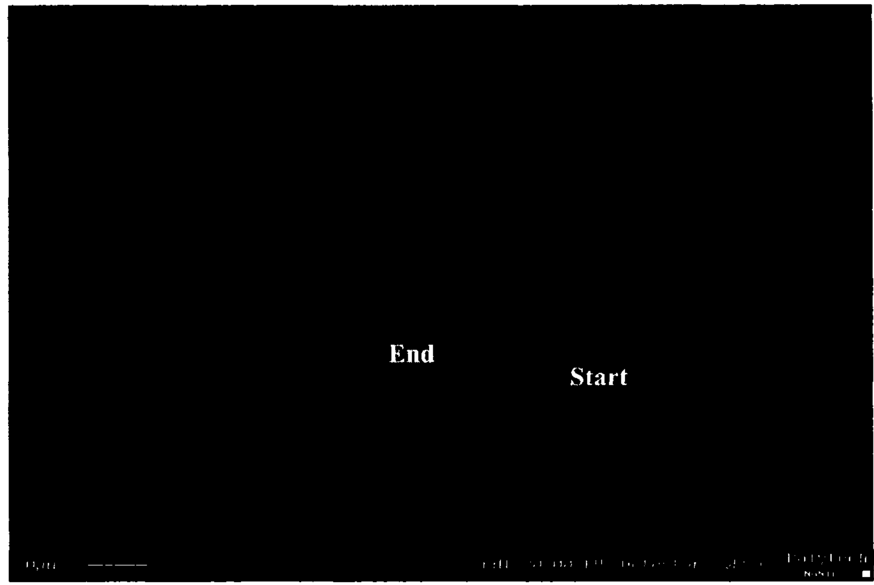

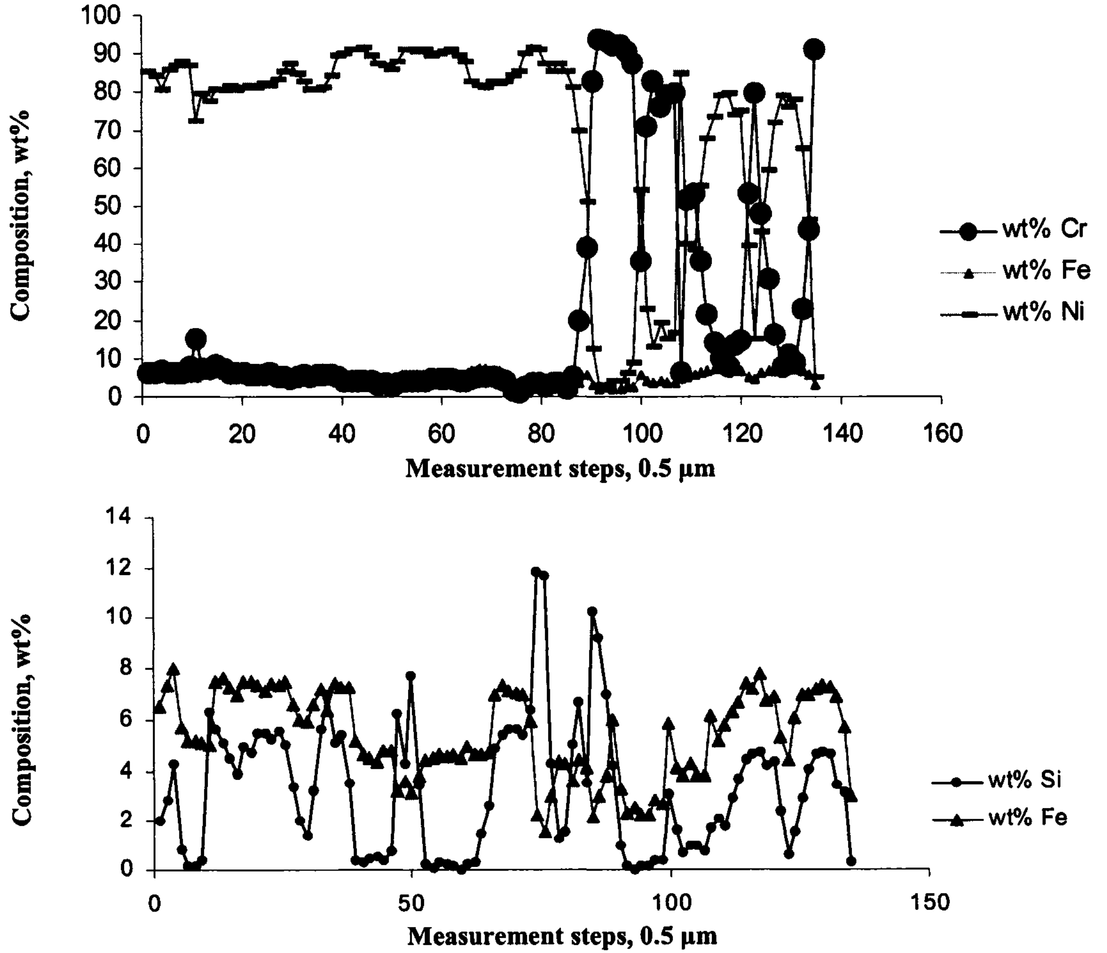

Fig. 5.10 Line scans through the centerline eutectics of an SS 410/BNi-2 joint brazed at 1325K for 50 minutes

5.2 Diffusion Induced Precipitation:

Conventional TLP models assume sequential liquid/solid equilibration and solid state diffusion of melting point depressants into the base alloy. Under these conditions, no boridic precipitation is expected in the base metal during the *TLP Bonding* process. However, because of rapid boron diffusion and its low solubility, parent metal close to the brazing gap was quickly oversaturated with boron which produced precipitation of boridic phases having a very dense arrangement as described in details in the previous section. This was evident in all brazed joints microstructures, irrespective of brazing temperature, holding time and joint gap. This suggests that diffusion of solute atoms into the base alloy could actually take place during base metal dissolution and liquid homogenization. Similar deviations from the conventional TLP models were reported by Gale and Wallach [92]. However, they proposed that these precipitations can be avoided if the operating temperature is set above the eutectic temperature of the *Ni-B* system. Because in that case, localized liquation of the substrate would take place and the liquid region would re-solidify following prolonged holding and would not result in the formation of persistent boridic phases. However, it is worth noting that they worked with pure nickel as the substrate and in the present study the base metals are complex multi-component alloys, therefore, although one of the bonding temperatures (1394K) was above the eutectic temperature of the binary *Ni-B* system, extensive boridic precipitations could not be avoided.

5.3 Dissolution of Base Alloy:

As described earlier, the fusing dissolution of base metal is inevitable during transient liquid phase bonding. The main beneficial aspect is that it can enhance the alloying process which in turn improves the mechanical properties of the brazed joints [29]. In this work, wedge-shape joint gap specimen model, as described in Chapter 4, was utilized to account for the dissolution of the base metal since the initial V-configuration is known. The dissolution of the base metal was calculated by measuring the final width of the brazement. Effect of holding time on the dissolution width of base metal at different bonding temperature is shown in Figure 5.11. Although the measured data were found to be scattered due to the physical and chemical uncertainties associated with TLP bonding experiments, it was obvious that dissolution is very rapid initially but quickly reaches the saturation limit at any selected bonding temperature. It was also observed that the saturated dissolution thicknesses of the base metal increased with increasing bonding temperatures.

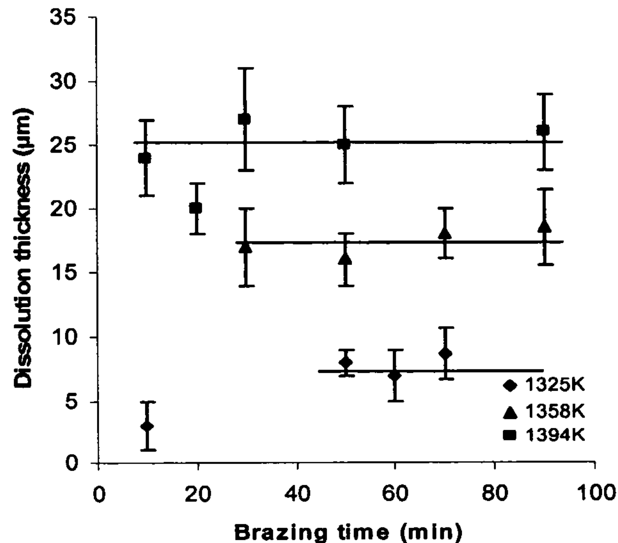

Fig. 5.11 Effect of bonding temperature and time on dissolution thickness of Inconel 718 base alloy for an initial joint gap of 75 μm

5.4 Maximum Brazing Clearances:

In the wedge gap brazed joint, a distinction is made between areas free of brittle phase and brittle phase containing seam sections. The beginning of brittle phase stabilization, as shown in Fig. 5.12, marks the maximum brazing clearance (MBC), after the corresponding dissolution width is subtracted, for the combination of base metals and filler alloy brazed at a particular temperature and holding time. Figures 5.13 (a) through (d) show the maximum brazing clearances for the Inconel 718/BNi-2, Inconel 625/BNi-2, SS 410/BNi-2 and SS 321/BNi-2 combinations, respectively, brazed at 1325K, 1358K and 1394K with different holding times ranged from 10 to 90 minutes. Conversely, if a specified MBC is taken, the corresponding brazing time will represent the isothermal solidification time for that brazing clearance. Therefore, experimental isothermal solidification time for a given process condition (initial joint gap and temperature) can be obtained from the corresponding best fitted line in the maximum brazing clearance diagram. It is also worth mentioning that significant reduction of holding time has been observed with increasing bonding temperature and/or decreasing joint gap.

Fig. 5.12 Micrograph showing the initiation of brittle eutectic phase (Inconel 718/BNi-2 joint brazed at 1394K for 50 minutes)

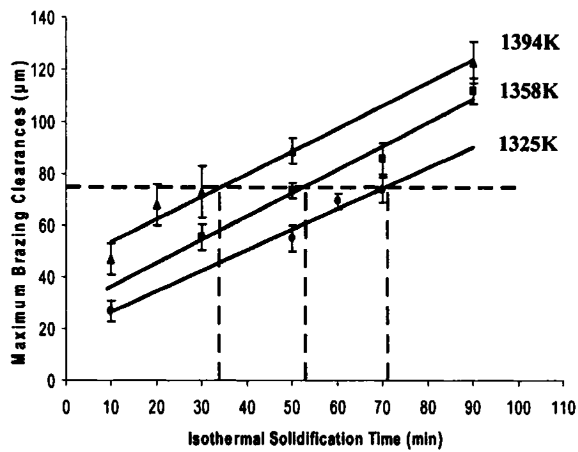

(a) Inconel 718/BNi-2

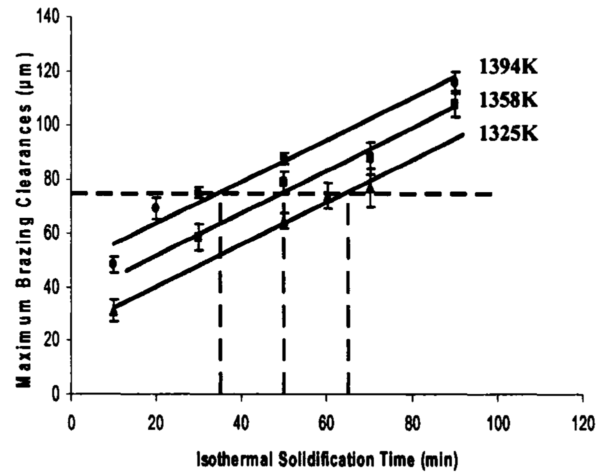

(b) Inconel 625/BNi-2

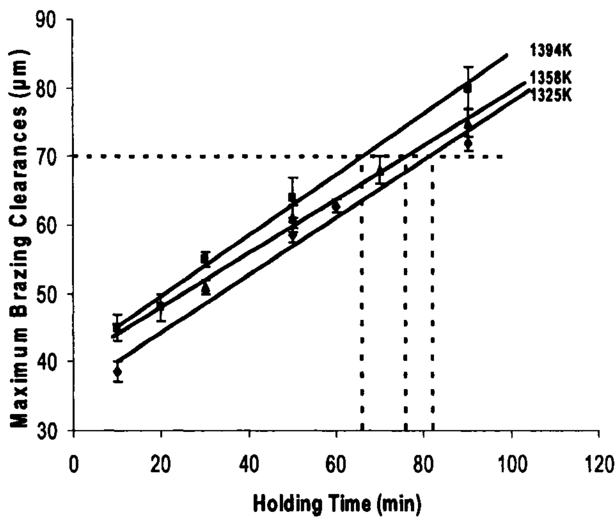

(c) SS 410/BNi-2

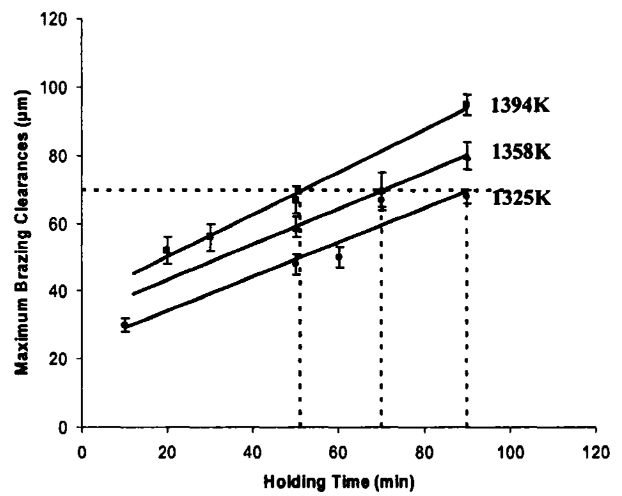

(d) SS 321/BNi-2

Fig. 5.13 Effect of holding time on the maximum brazing clearances of (a) Inconel 718/BNi-2, (b) Inconel 625/BNi-2, (c) SS 410/BNi-2 and (d) SS 321/BNi-2

Chapter 6

Mathematical Modeling and Methodology

6.1. Random Walk Modeling Based on Migrating Solid/Liquid Interface:

The *migrating solid/liquid interface model* takes into consideration the moving solid/liquid interface as described in chapter 2. Moreover, it is coupled with experimental isothermal solidification times to obtain the diffusion coefficients of solute atoms into the base alloys being used. However, there are several physical and chemical uncertainties associated with the experimental investigations which directly affect the kinetics of the diffusion process, and no single value of diffusion coefficient would be representative for real life *TLP Bonding* experiments. Physical uncertainties include, but are not limited to, (i) variation of nickel layer thickness in the base alloy after nickel flushing, (ii) waviness of the faying surface, (iii) uncertainties in temperature, time and length measurements, (iv) variation of joint configurations, (v) heterogeneous wetting of base alloy by the filler alloy, etc. Chemical uncertainties include, but are not limited to, (i) compositional variations of solute atoms in the filler alloy throughout the joint gap, (ii) heterogeneity in the elemental composition of the base alloys etc. These uncertainties directly affect the assumption of unidirectional diffusion of solute atoms. Therefore, it is quite obvious that diffusion of solute atoms cannot be modeled assuming an ideal case to predict the time required for complete isothermal solidification; rather, it should be modeled taking the random diffusion of solute atoms into considerations due to the physical and chemical

uncertainties associated with transient liquid phase bonding experiments. However, the random numbers should be based on the type of statistical distribution, such as normal, weibull, uniform distribution etc., being observed for diffusion coefficients, obtained from experimentally determined isothermal solidification times, and by taking the mean and standard deviation into considerations. Therefore, such random numbers are based on logical reasoning.

6.1.1 Calculation of Diffusion Coefficients:

Ideally, diffusion coefficient of solute atoms at a specified bonding temperature is constant. However, as described earlier, a constant diffusion coefficient at the bonding temperature is not representative of what is practically encountered during the *TLP Bonding* process. A range of diffusion coefficients can be obtained for each of the three bonding temperatures by substituting several experimentally obtained post-brazed maximum clearances free of eutectic phases and the corresponding holding times in equation (2.16). Diffusion coefficient of solute atom into the base alloy can then be modeled as a random number, which can be generated using the MATLAB Random Number Generation function, based on the type of statistical distribution being observed, and by taking the mean and standard deviation into consideration.

6.1.2 Modified Model Equations:

The model equations are thus modified as following:

$$D_{i,j} = \frac{(2h_{i,j})^2}{16\gamma^2 t_{i,j}} \qquad (6.1)$$

where i = 1, 2, 3… n, which denotes the number of experimentally determined post-brazed maximum joint widths free of eutectic phases and the corresponding holding times for each bonding temperature.

j = 1325K, 1358K, 1394K, which denotes the bonding temperature.

Diffusion coefficient at a specified bonding temperature can then be written as:

$$D_j = [D_{1,j}, D_{2,j}, D_{3,j} ....D_{n,j}] \quad (6.2)$$

If diffusion of solute atoms is modeled as a random number, based on the statistical distribution profile of D_j being observed, diffusion coefficient for a specified bonding temperature can be written as following:

$$D_{R(j)} = R_{D_j} \quad (6.3)$$

where R_{D_j} is a random number based on the statistical distribution profile of D_j, as described before.

Isothermal solidification times for a given process condition can then be calculated using the following relation:

$$t_{f_{i,j}}^{1/2} = \frac{1}{4\gamma}\left(\frac{2h_{i,j}}{D_{R(j)}^{1/2}}\right) \quad (6.4)$$

6.2 Random Walk Modeling Based on Solute Distribution Law:

Although *solute distribution model* is a simple modeling approach which does not take into consideration the dissolution of base metal, sometimes it can be very useful to have a reasonable approximation of holding time required to complete isothermal solidification.

Similar approach has been used to modify the *solute distribution model* equations. Since the initial composition of boron in both Inconel 718 and 625 superalloys and SS 410 and SS 321, $C_m = 0$, equation (2.9) can be modified as following:

$$D_{i,j} = \frac{w_{i,j}^{\;2}}{\left(erf^{-1}\left(\frac{C_s}{C_0}\right) \right)^2 * 4 * t_{i,j}} \quad \ldots\ldots\ldots\ldots\ldots\ldots\ldots (6.5)$$

where $w_{i,j}$ are the halves of the maximum brazing clearances obtained experimentally for each bonding temperature and $t_{i,j}$ are the corresponding holding times.

The isothermal solidification times for a given process condition can then be predicted using the following equation:

$$t_{f_{i,j}} = \frac{w^2}{\left(2 * erf^{-1}\left(\frac{C_s}{C_0}\right) * \sqrt{R_{D_j}}\right)^2} \quad \ldots\ldots\ldots\ldots\ldots\ldots\ldots (6.6)$$

where w is half of the initial joint gap thickness for which the isothermal solidification time is to be calculated.

6.3 Summary of the Proposed Methodology:

TLP Bonding experiments using wedge-shape joints enable to determine maximum brazing clearances and, thus, the ranges of apparent diffusion coefficients for different bonding temperatures using migrating solid/liquid interface and solute distributions models. Isothermal solidification times for different process conditions can then be predicted using Random Walk Modeling and verified with the experimentally determined values. Following flow chart illustrates the methodology used in the current study:

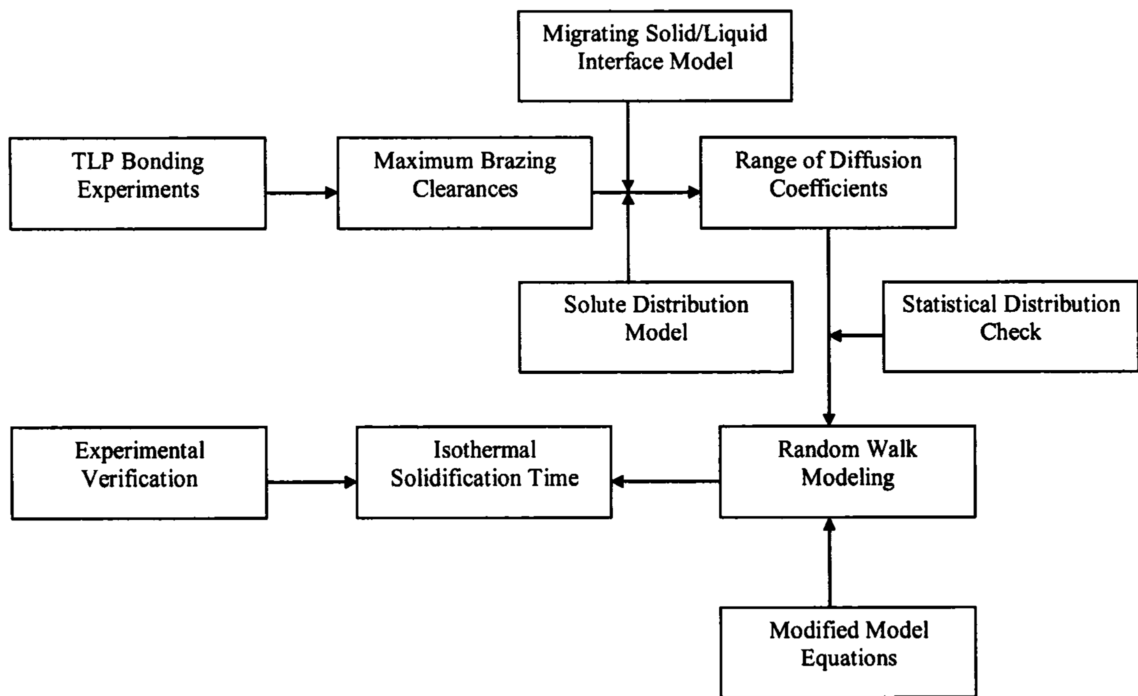

Fig. 6.1 Flow chart illustrating the methodology of the current study

Chapter 7

Results and Discussions

Both modified migrating solid/liquid interface and solute distribution models have been applied, taking the random diffusion of solute atoms into consideration, to predict the isothermal solidification times during *TLP Bonding* of Inconel 718 and 625, and SS 410 and 321 with nickel based filler alloy BNi-2.

7.1 Inconel 718/BNi-2 and Inconel 625/BNi-2:

7.1.1 Migrating Solid/Liquid Interface Model:

Boron has very low solubility in nickel. Previous investigation [2] on *TLP Bonding* of nickel superalloy, Inconel 738, with nickel based filler alloy, Nicrobraz 150, have suggested that the presence of additional alloying elements does not change the $C_{\alpha L}$ and $C_{L\alpha}$ values significantly from those of the *Ni-B* system. Similar approach was also used by other researchers [7,18,108]. Therefore γ, the parameter for moving boundary, was calculated by taking $C_{\alpha L}$ and $C_{L\alpha}$ as the average solidus and liquidus boron compositions of the *Ni-B* system at the bonding temperature range, 0.3 at% and 16.6 at%, respectively.

Range of diffusion coefficients for each of the three bonding temperatures have been obtained using 28 sets of experimentally determined post-brazed maximum clearances free of eutectic phases and the corresponding holding times and are presented in Tables 7.1 and 7.2 for Inconel 718/BNi-2 and Inconel 625/BNi-2, respectively. The

ratios of standard deviations to the mean values at 1358K were found to be smaller than those of the other two bonding temperatures. It suggests that the experimental data can be considered less scattered at this temperature. A narrower prediction range of isothermal solidification times is thus expected at 1358K than the other two temperatures. It was found that the distribution profiles of diffusion coefficients were almost always normal, such as Fig. 7.1, and only in few cases deviated from normality towards weibull.

Table 7.1 Range of diffusion coefficients obtained from experimentally determined isothermal solidification times for Inconel 718/BNi-2 combination

Bonding Temp. (K)	Diffusion Coefficients (m^2s^{-1}) x 10^{-10}			
	D_{min}	D_{max}	Mean	STDV
1325	5.82	7.7	6.99	0.84
1358	14.4	17.6	15.5	1.4
1394	22.3	33.6	28.2	5.27

Table 7.2 Range of diffusion coefficients obtained from experimentally determined isothermal solidification times for Inconel 625/BNi-2 combination

Bonding Temp. (K)	Diffusion Coefficients (m^2s^{-1}) x 10^{-10}			
	D_{min}	D_{max}	Mean	STDV
1325	8.43	13.05	10.54	1.05
1358	14.4	18.07	16.5	1.62
1394	21.5	39.5	31.2	8.3

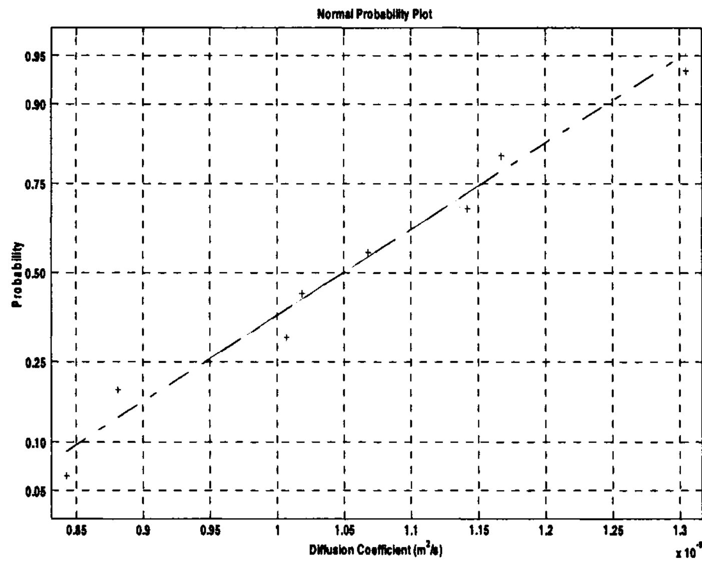

Fig. 7.1 Example of normality check of diffusion coefficient (Inconel 625/BNi-2 combination at 1325K bonding temperature)

Numerical simulations were carried out with modified model equations as given earlier. Figures 7.2 (a) and (b) show the cumulative probability and probability density of isothermal solidification time for Inconel 718/BNi-2 and Inconel 625/BNi-2 combinations, respectively, for an initial joint gap of 75 μm at 1358K bonding temperature. Isothermal solidification time for the process condition has been predicted as a range where different values have different individual probabilities. Cumulative probability distribution is a very useful tool because it can be interpreted as the probability that isothermal solidification will take place for less than or equal to a given holding time, e.g. a holding time of 60 minutes would include the probabilities of isothermal solidification times that are less than or equal to 60 minutes. Therefore, it is a measure of the confidence level that isothermal solidification would take place if the

corresponding length of time is elapsed in the furnace at the bonding temperature. This is also very significant from industrial point of view. For the assembly that requires a high safety factor, isothermal solidification time should be considered as the one that corresponds to a very high CP value, close to 1, to eliminate any possibility of failure due to the formation of brittle eutectic phases.

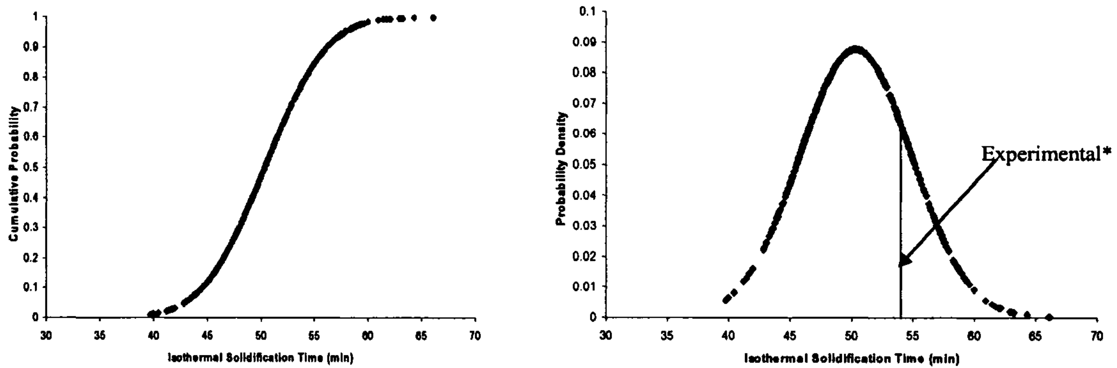

(a) Inconel 718/BNi-2

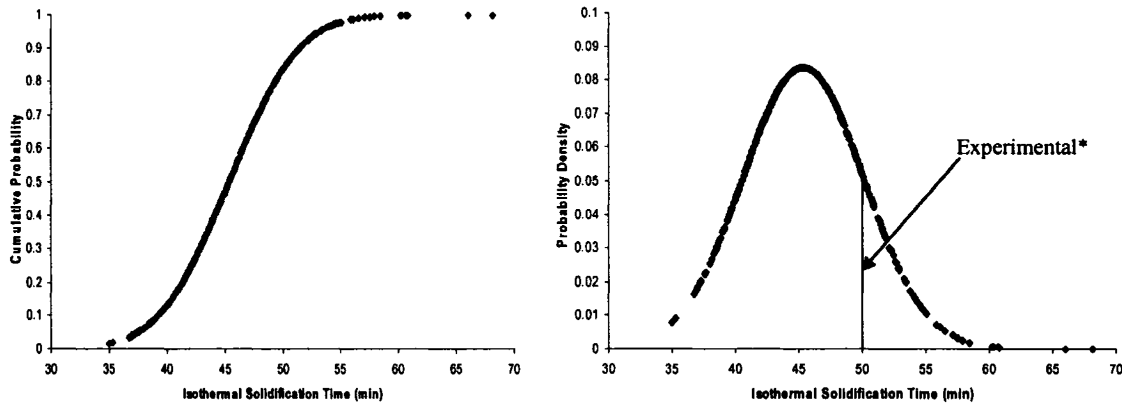

(b) Inconel 625/BNi-2

Fig. 7.2 Cumulative probability plot and probability density plot of isothermal solidification time for (a) Inconel 718/BNi-2 and (b) Inconel 625/BNi-2 for an initial joint gap of 75 μm and 1358K bonding temperature [* experimental data have been obtained from the best fitted lines of the maximum brazing clearance diagrams: Fig. 5.13 (a) and (b), respectively]

The predicted isothermal solidification times for three different bonding temperatures, with different confidence levels, have been compared with experimentally determined values, as shown in Fig. 7.3. It should be noted here that a lower confidence level, such as 50% CP, is not an indication that the probability of occurrence of that event is lower than that of a higher confidence level. In fact, for a perfectly normal distribution, 50% confidence level values have the highest individual probability.

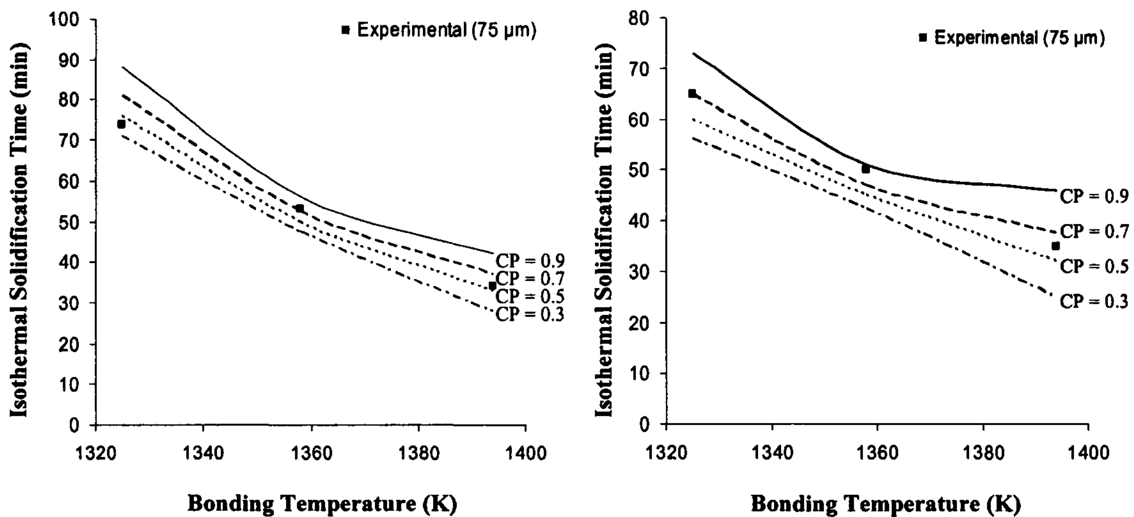

Fig. 7.3 Comparison of predicted isothermal solidification times with different confidence levels (migrating solid/liquid interface model) with experimental data for an initial joint gap of 75 μm for (a) Inconel 718/BNi-2 and (b) Inconel 625/BNi-2 [CP = Cumulative Probability (a measure of the confidence level)]

As evident from Fig. 7.3, the model predicted the isothermal solidification times reasonably well. It should be noted here that the experimental values were extracted from the best fitted line in the maximum brazing clearance diagrams (Fig. 5.13(a) and (b)). For

each combination of base and filler alloy, only one experimental isothermal solidification time can be obtained for each of the bonding temperatures for a given joint gap. For statistical validation purpose, more experimental data of the same process condition are recommended. However, it requires extensive repetition of braze test matrix (Table 4.2) which was beyond the scope of the present investigation. However, the model was further verified for an initial joint gap of 85 μm which also showed very good agreement with the experimental data, e.g. Fig. 7.4.

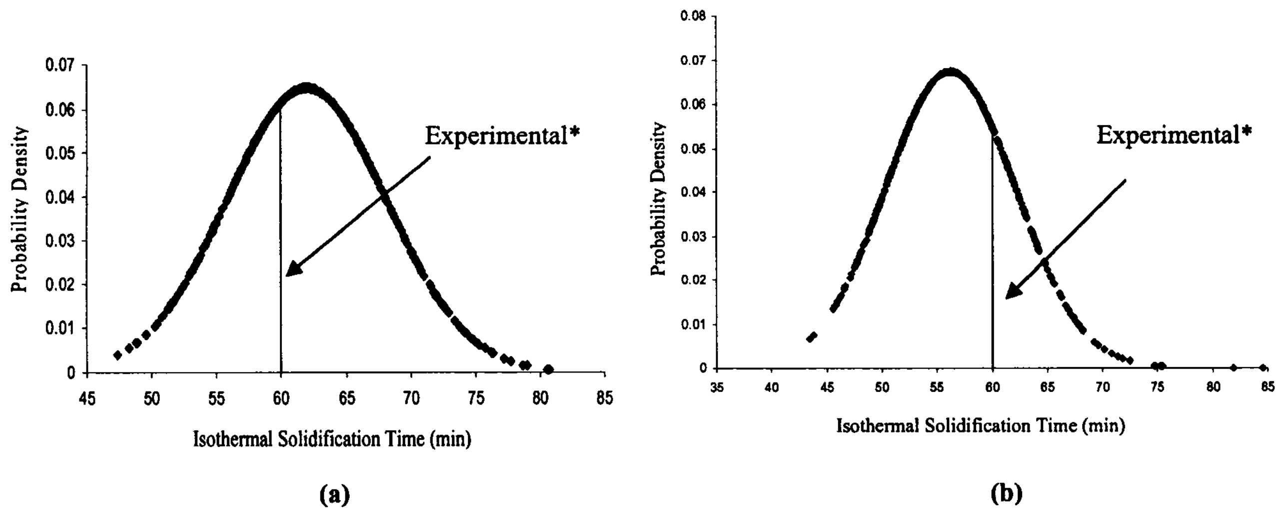

Fig. 7.4 Model verification for 85 μm joint gap at 1358K: (a) Inconel 718/BNi-2 and (b) Inconel 625/BNi-2 [*obtained from Fig. 5.13 (a) and (b), respectively]

7.1.2 Solute Distribution Law Approach:

Similar studies were carried out for the solute distribution modeling approach. The value of C_s was taken as 0.3 at% following the reasons described in section 7.1.1. The predicted isothermal solidification times with different confidence levels, for an initial joint gap of 75 μm and for three different operating temperatures, are compared with

experimental data in Fig. 7.5. It was observed that unlike migrating solid/liquid interface model, solute distribution model is underestimating the isothermal solidification times at higher temperature bonding operation for both of the combinations. This can be attributed to the fact that solute distribution model does not take into consideration the dissolution of base metal which is significant at higher temperature. It can, therefore, be inferred that although this simple model can be used for a reasonable approximation of isothermal solidification time, migrating solid/liquid interface model should be used for better accuracy and reliability.

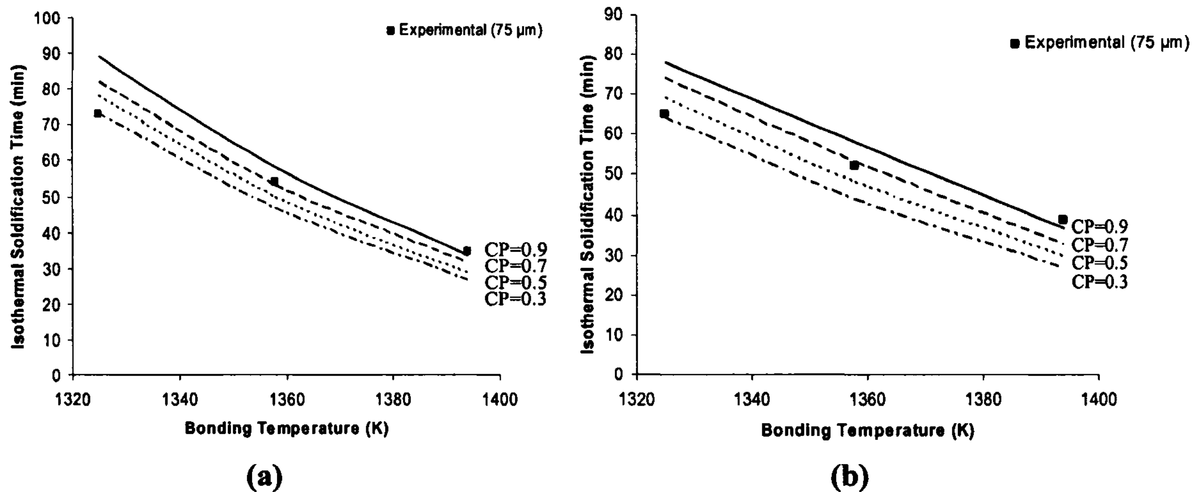

Fig. 7.5 Comparison of predicted isothermal solidification times with different confidence levels (solute distribution model) with experimental data for an initial joint gap of 75 μm for (a) Inconel 718/BNi-2 and (b) Inconel 625/BNi-2 [CP = Cumulative Probability (a measure of the confidence level)]

7.2 SS410/BNi-2 and SS 321/BNi-2:

7.2.1 Migrating Solid/Liquid Interface Model:

Range of diffusion coefficients for each of the three bonding temperatures have been obtained using 28 sets of experimentally determined post-brazed maximum clearances free of eutectic phases and the corresponding holding times and are presented in Tables 7.3 and 7.4 for SS 410/BNi-2 and SS 321/BNi-2, respectively. Like the superalloy combinations, the ratios of standard deviations to the mean values were found to be much smaller at 1358K than those of the other two bonding temperatures and, therefore, much narrower prediction ranges of isothermal solidification times are expected at this temperature. The modified migrating solid/liquid interface model has been applied to predict the isothermal solidification time for an initial joint gap of 70 μm and for three different operating temperatures.

Table 7.3 Range of diffusion coefficients obtained from experimentally determined isothermal solidification times for SS 410/BNi-2 combination

Bonding	Diffusion Coefficients (m^2s^{-1}) x 10^{-10}			
Temp. (K)	D_{min}	D_{max}	Mean	STDV
1325	5.40	13.76	7.93	3.92
1358	7.29	9.26	8.13	0.86
1394	10.59	20.34	13.49	3.92

Table 7.4 Range of diffusion coefficients obtained from experimentally determined isothermal solidification times for SS 321/BNi-2 combination

Bonding	Diffusion Coefficients (m^2s^{-1}) x 10^{-10}			
Temp. (K)	D_{min}	D_{max}	Mean	STDV
1325	4.81	10.38	6.95	2.63
1358	9.07	10.8	9.83	1.58
1394	10.44	16.0	12.79	2.4

Figures 7.6 (a) and (b) show the cumulative probability distribution and probability density plots for holding time required to complete isothermal solidification at 1358K bonding temperature with 70 μm initial joint gap for SS 410/BNi-2 and SS 321/BNi-2, respectively. Like nickel superalloy combinations, the isothermal solidification times have been predicted as a range where different values have different individual probabilities. Predicted isothermal solidification time for different confidence levels were compared with experimental data for both of the two combinations, as shown in Fig. 7.7. It was interesting to observe that for SS 410/BNi-2, the model underestimated the time requirement at higher temperature bonding operations (1358K and 1394K) which suggests that the solubility limit of boron might have decreased. This can be attributed to the following model assumption: the value of $C_{\alpha L}$ and $C_{L\alpha}$ were taken as 0.3 at% and 16.6 at %, respectively, which are the average solidus and liquidus boron compositions in the *Ni-B* system at the bonding temperatures. This assumption is reasonable when the base metals are pure nickel or nickel based superalloys. However, when stainless steels, such as SS 410, are used as base metals, significant amount of iron dissolves into the joint due to the dissolution of base metal, especially at higher bonding temperatures; and the assumptions of 0.3 at% solubility and 16.6 at% liquidus composition are no longer appropriate. A decrease of solubility limit ($C_{\alpha L}$) or an increase of liquidus composition ($C_{L\alpha}$) would result in an underestimation of the time requirement to complete isothermal solidification. The effect of solubility limit is much higher than that of the liquidus composition. The maximum solubility of boron in iron is 0.1 at% [109] which is one third of that in nickel. Decreased solubility limit of boron in the multi-component melt at higher operating temperature is, thus, justified.

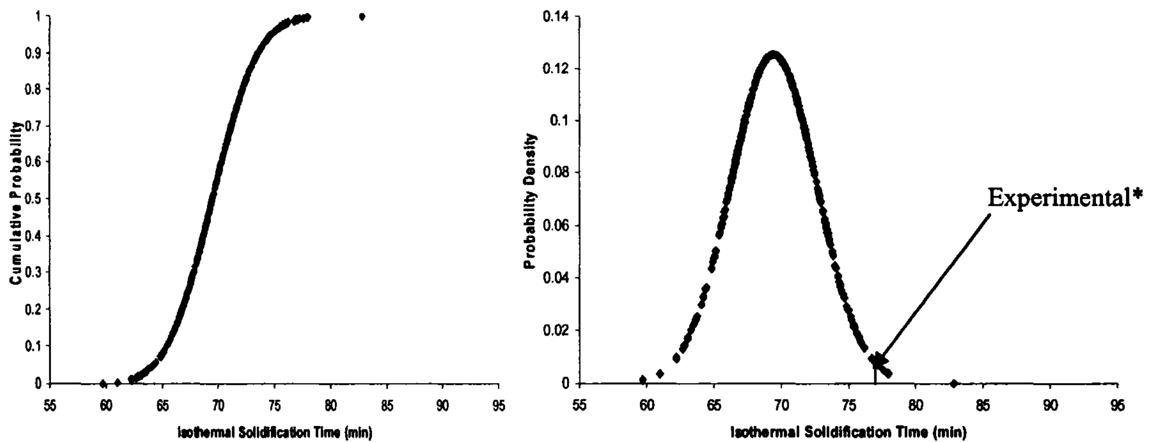

(a) SS 410/BNi-2

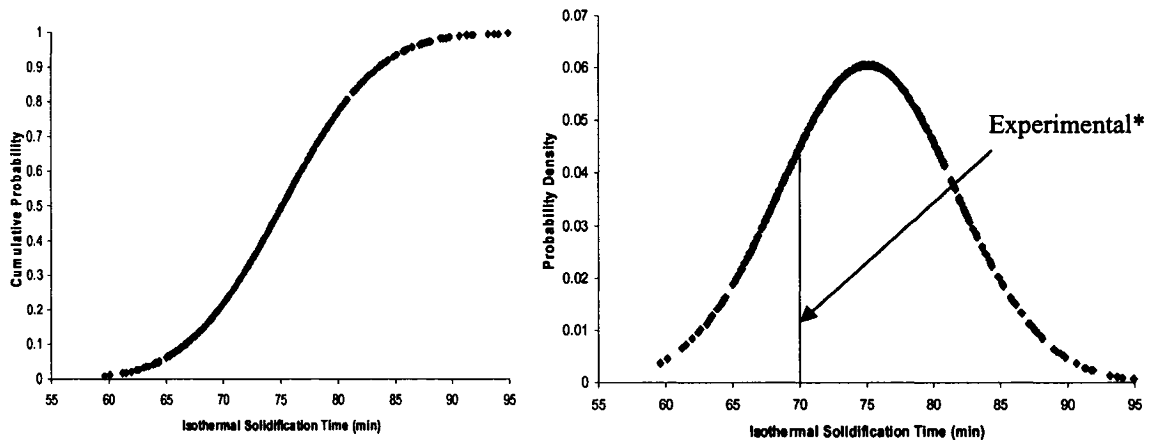

(b) SS 321/BNi-2

Fig. 7.6 Cumulative probability plot and probability density plot of isothermal solidification time (migrating solid/liquid interface model) for (a) SS 410/BNi-2 and (b) SS 321/BNi-2 for an initial joint gap of 70 μm and 1358K bonding temperature [* experimental data have been obtained from the best fitted lines of the maximum brazing clearance diagrams: Fig. 5.13 (c) and (d), respectively]

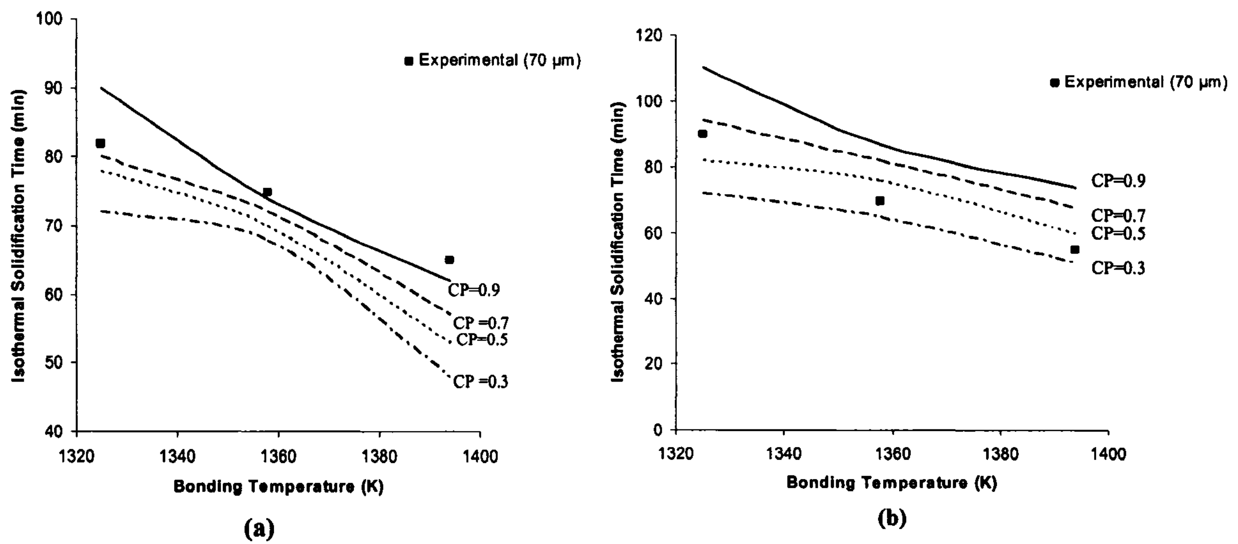

Fig. 7.7 Comparison of predicted isothermal solidification times with different confidence levels (migrating solid/liquid interface model) with experimental data for an initial joint gap of 70 µm for (a) SS 410/BNi-2 and (b) SS 321/BNi-2

To verify this reasoning, the model was run for a solubility limit of 0.2 at% for both 1358K and 1394K bonding temperatures which showed very good agreement with the experimentally determined values, as shown in Fig. 7.8. For further verification, the model was also run for 80 µm initial joint gap for both 0.3 at% and 0.2 at% boron solubility and compared with the experimentally determined values, e.g. Fig. 7.9. Again, the model underestimated the isothermal solidification time when 0.3 at% solubility was used whereas very good agreement was observed for 0.2 at%. Therefore, it can be inferred that 0.3 at% solubility can be used to predict the isothermal solidification time requirement at low temperature bonding operation; however, for higher operating

temperatures (1358K – 1394K) reduced boron solubility should be used for better prediction of isothermal solidification time.

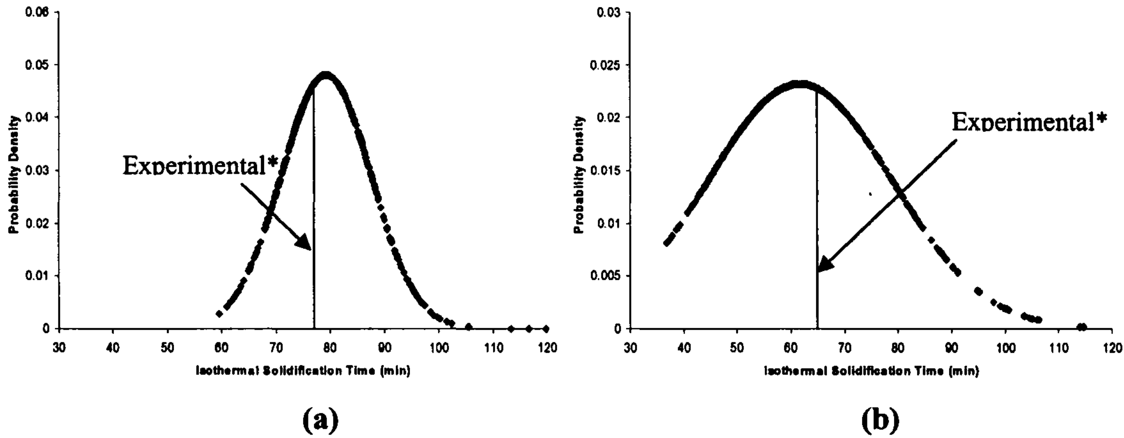

(a) (b)

Fig. 7.8 Verification of decreased boron solubility (0.2 at%) for SS 410/BNi-2 combinations with an initial joint gap of 70 μm for (a) 1358K and (b) 1394K [* obtained from Fig. 5.13 (c)]

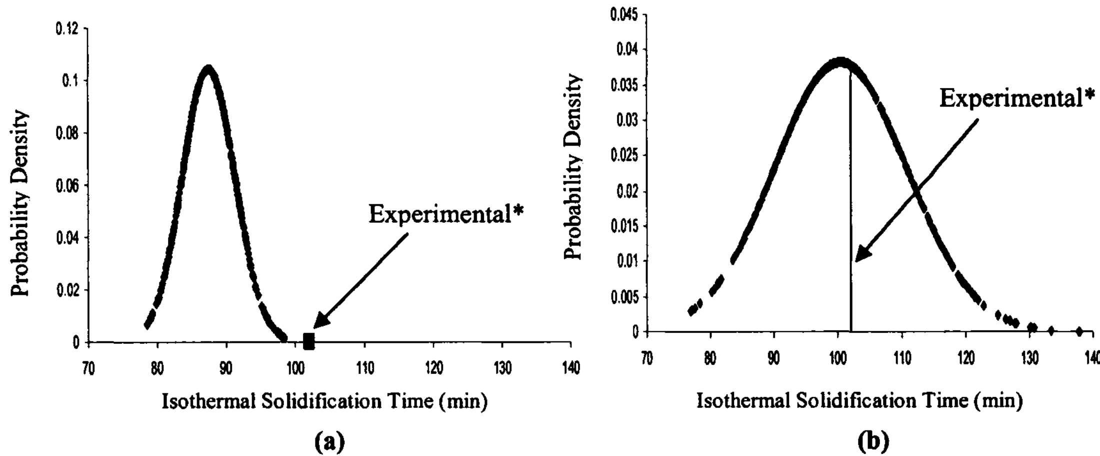

Fig. 7.9 Verification of decreased boron solubility for SS 410/BNi-2 at 1358K with an initial joint gap of 80 μm: (a) 0.3 at% and (b) 0.2 at% [* obtained from Fig. 5.13 (c)]

It was interesting to observe that, unlike SS 410/BNi-2 combination, the predicted isothermal solidification times for SS 321/BNi-2 were in good agreement with

experimentally determined values in the temperature range being investigated although the maximum probability densities were found to be much smaller than those of SS 410/BNi-2 which resulted into wider prediction ranges of isothermal solidification times. To verify this observation further, the predicted isothermal solidification times for 80 μm initial joint gap were compared with experimental data which also showed very good agreement, e.g. Fig. 7.10.This suggests that the assumptions of $C_{\alpha L}$ = 0.3 at% and $C_{L\alpha}$ = 16.6 at% are applicable for SS 321/BNi-2 combination. This can be attributed to the fact that unlike SS 410, the amount of nickel and chromium is significant in austenitic stainless steel SS 321, 12 wt% and 19 wt%, respectively, whereas in SS 410, these amounts are 0.75 wt% and 12 wt%, respectively. Although dissolution of base metal brought some iron into the melt, its concentration in the melt is much smaller than that of SS 410 base alloy. Therefore, it can be inferred that the amounts of nickel and chromium in the base metal, as low as 12 wt% and 19 wt%, respectively, can mitigate the effect of iron on the validity of the assumption of 0.3 at% boron solubility. The solubility limit (C_s = 0.3 at%) will be further verified later with solute distribution model.

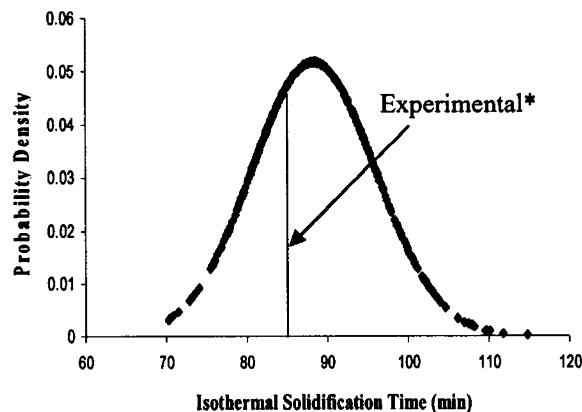

Fig. 7.10 Verification of 0.3 at% boron solubility for SS 321/BNi-2 combination for an initial joint gap of 80μm at 1358K [*obtained from Fig. 5.13 (d)]

7.2.2 Solute Distribution Modeling Approach:

Figure 7.11 shows the predicted isothermal solidification times for both SS 410/BNi-2 and SS 321/BNi-2 combinations. Results are quite good for the SS 321/BNi-2 combination but the isothermal solidification times were underestimated at 1358K and 1394K for SS 410/BNi-2 combination. This was also observed in migrating solid/liquid interface model and confirms the hypothesis of decreased boron solubility at higher bonding temperatures.

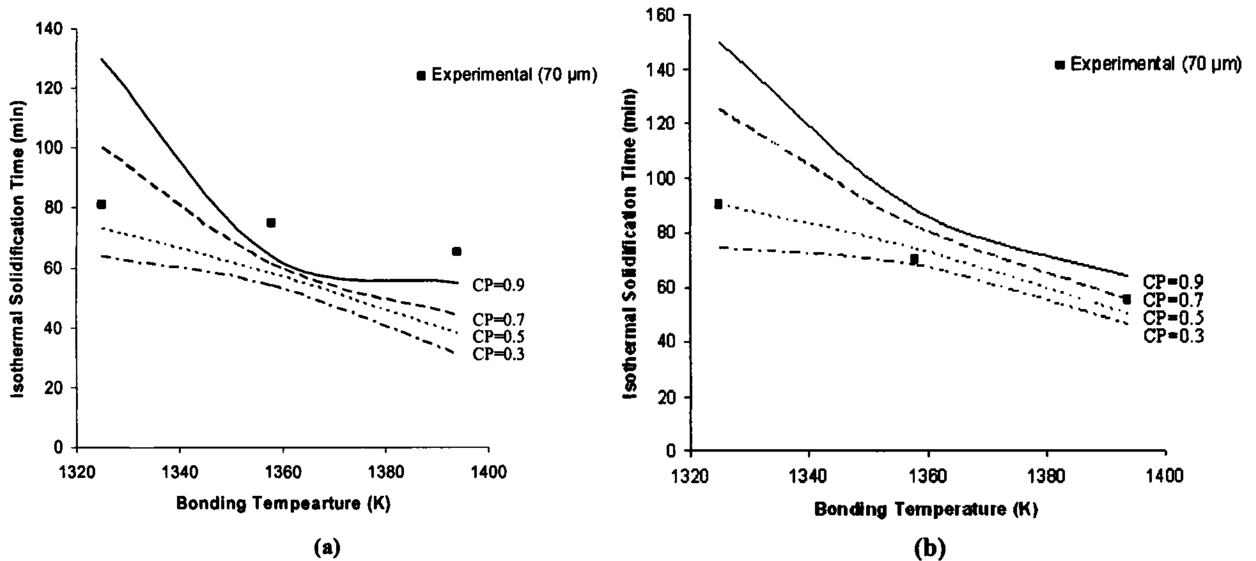

Fig. 7.11 Comparison of predicted isothermal solidification times with different confidence levels (solute distribution model) with experimental data for an initial joint gap of 70 μm for (a) SS 410/BNi-2 and (b) SS 321/BNi-2

The simulation results were extended for a solubility limit of 0.2 at% for the 1394K bonding temperature, as shown in Fig. 7.12. Similar to the solute distribution simulation results of nickel superalloys, the predicted values are underestimated compared to that of

the migrating solid/liquid interface model as evident from the large distance between the experimentally determined value and the predicted maximum probability density. The same reasoning of not accounting for the dissolution thickness can be given.

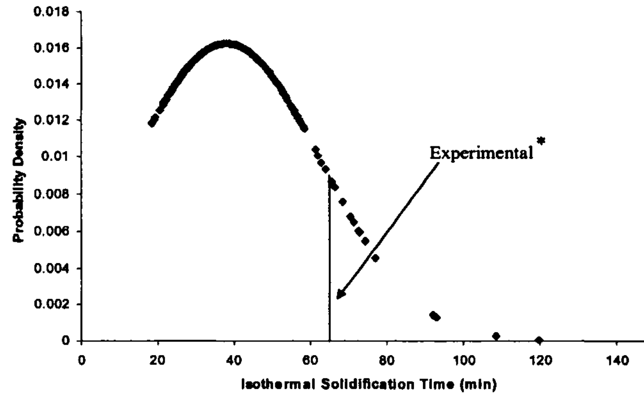

Fig. 7.12 Verification of 0.2 at% solubility limit for SS 410/BNi-2 using solute distribution model for 1394K temperature with an initial joint gap of 70 μm [*obtained from Fig. 5.13 (c)]

Unlike SS 410/BNi-2 combination, the predicted isothermal solidification times for SS 321/BNi-2 combination were in good agreement in the temperature range being investigated which was also the case with the migrating solid/liquid interface model. This, again, suggests that the assumption of 0.3 at% solubility is reasonable for SS 321/BNi-2 combination.

7.2.3 Silicon diffusion model for SS 410/BNi-2:

As mentioned earlier, due to the dissolution of base metal, significant amount of iron comes into play during the *TLP Bonding* of SS 410/BNi-2 combination. Therefore, taking the boron solubility from the *Ni-B* binary system as a reference to form solid

solution is not likely to be appropriate for this system. Like boron, silicon also acts as a melting point depressant which diffuses out from the joint towards the base metal. From the EDS analyses of Fig. 5.7, the average silicon composition in the isothermally solidified joint area adjacent to the solid/liquid interface was found to be ≈ 3.16 wt%. Modified solute distribution model equations were then used to predict the times requirement to complete isothermal solidification for an initial joint gap of 70 μm in the similar way as it was done for boron diffusion model.

Figure 7.13 shows the predicted isothermal solidification times with different confidence levels based on silicon diffusion model in relation to the experimental data. The reference solubility to form *γ-nickel* solid solution need not be assumed for silicon diffusion model and that is why the predicted isothermal solidification times were in better agreement than the other models that rely on the assumption of 0.3 at% boron solubility.

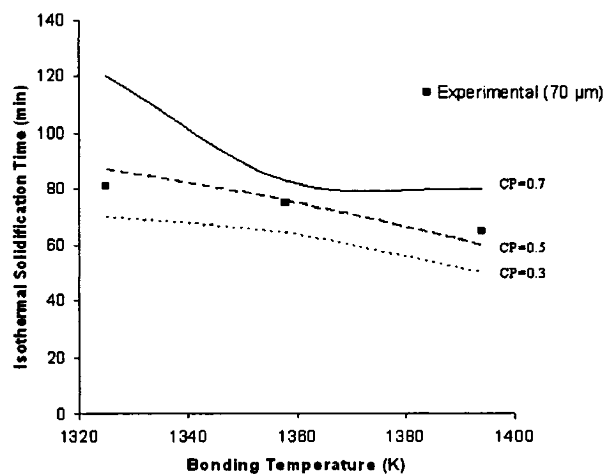

Fig. 7.13 Comparison between the predicted isothermal solidification times with different confidence levels (silicon diffusion model based on solute distribution law) and the experimental data for an initial joint gap of 70 μm for SS 410/BNi-2

Chapter 8

Summary and Conclusions

8.1 Summary and Conclusions:

A comprehensive study of isothermal solidification during *Transient Liquid Phase (TLP) Bonding* of nickel based polycrystalline superalloys, Inconel 718 and 625, stainless steels 410 and 321 with nickel based filler alloy, BNi-2, have been carried out using mathematical modeling and experimental investigations.

In contrary to the conventional *TLP models*, extensive volume and grain boundary precipitations were observed in all brazed joint samples. Therefore, it is quite obvious that diffusion of solute atoms into the base alloys actually takes place during base metal dissolution and liquid homogenization.

The kinetics of isothermal solidification during *TLP Bonding* has been studied through migrating solid/liquid interface modeling and solute distribution law. However, unlike conventional modeling approaches, the apparent diffusion of solute atoms have been modeled using the Random Walk Modeling technique which can take into account the physical and chemical uncertainties associated with *TLP Bonding* experiments. The modified model equations for both modeling approaches have been developed and presented in this dissertation.

The concept of cumulative probability distribution and probability density plots of isothermal solidification times were introduced. Predicted isothermal solidification times

for various process conditions with different confidence levels were compared with experimental data. It was found that although the modified solute distribution model is useful to estimate the isothermal solidification time reasonably, modified migrating solid/liquid interface model is more reliable and accurate.

Unlike other currently used nickel superalloy combinations, the isothermal solidification completion times for Inconel 718 and 625 with BNi-2 filler alloy were found to be much shorter. It was also observed that although the isothermal solidification times of SS 410/BNi-2 and SS 321/BNi-2 combinations were relatively higher than those of nickel superalloy combinations, they were significantly less than those of other stainless steels with different nickel based filler alloys reported in the literature. Further significant reduction of holding time was observed with increasing bonding temperature and/or decreasing joint gap thickness.

Both migrating solid/liquid interface model and solute distribution model have underestimated the time requirement to complete isothermal solidification for SS 410/BNi-2 combination at higher temperature bonding operations (1358K – 1394K) which suggests that the solubility limit of boron has decreased in this temperature range. In this study, 0.2 at% solubility was used for the abovementioned temperature range and good agreement was observed with experimental data. The isothermal solidification times predicted by silicon diffusion model were in reasonable agreement with the experimental data because it does not rely on the assumption of reference solubility to form *γ-nickel* solid solution.

Unlike SS 410/BNi-2 combination, the predicted isothermal solidification times for the SS 321/BNi-2 combination, by both migrating solid/liquid interface and solute

distribution models, were in good agreement with the experimentally determined values. It can, therefore, be concluded that the amount of nickel, as low as 12 wt%, and the amount of chromium, as low as 19 wt%, can mitigate the effect of iron, on the validity of the assumption of solubility limit and liquidus composition of boron, that comes into the melt due to the dissolution of base alloy.

8.2 Contributions:

The kinetics of isothermal solidification during transient liquid phase bonding of Inconel 718, Inconel 625, SS 410 and SS 321 with nickel based filler alloy BNi-2 have been studied for the first time.

Experimental investigations have been carried out over a wide range of bonding temperature and joint gaps. Maximum brazing clearance diagrams, very useful way to determine isothermal solidification times when the process conditions are varied, have been obtained for each of the four combinations. These will also serve as a reference for any future modeling studies.

Unlike conventional modeling, the diffusion of solute atoms into the base alloys have been modeled using the Random Walk Modeling technique which can take into account the physical and chemical uncertainties associated with transient liquid phase bonding experiments. By using the concept of apparent diffusion coefficients, model equations for both migrating solid/liquid interface and solute distribution law have been modified and presented.

It has been found that the isothermal solidification times for Inconel 718/BNi-2 and Inconel 625/BNi-2 are much less than many other currently used combinations.

Isothermal solidification times for the stainless steel combinations were also found to be reasonably less than other stainless steel combinations with different nickel based filler alloys. This is a very significant finding from practical point of view because *TLP Bonding* community has been searching for suitable combinations of base and filler alloys that can offer reasonably low isothermal solidification time.

It was shown in this study that conventional modeling approach of 0.3 at% solubility of boron as a reference to form solid solution is not appropriate for stainless steels with high iron content such as SS 410, especially at higher bonding temperatures. The appropriate solubility has been determined for the first time.

It was also presented in this study that silicon, which also acts as a melting point depressant in nickel based filler alloys, can be used as a reference element in the mathematical models to determine the time required to complete isothermal solidification

8.3 Future Research Directions:

Considerable reduction of time required to complete isothermal solidification has been observed with the increase of bonding temperature and/or with the decrease of initial joint gap. However, when the material limits the temperature and the complex geometry does not allow the joint gap to be narrow enough to have a reduced isothermal solidification time; it is necessary to predict the extent of formation of brittle eutectic phases. Computational thermodynamics, using a multi-component thermodynamic database, coupled with kinetic model of diffusion can be applied to predict the amount of these deleterious phases evolved from the residual liquid when the holding time is not long enough to complete isothermal solidification. It should be noted here that commercial databases do not cover the whole composition range that is encountered

during the TLP bonding process and development of such thermodynamic database is absolutely vital for predicting the final joint microstructures and also for filler alloy developments.

Effect of surface preparation plays a significant role during the process kinetics of TLP bonding since it can expedite or slow down the diffusion of melting point depressant into the base alloy. Detail investigations of TLP bonded samples with different surface preparations will enable better understanding of the diffusion phenomenon and, optimum technique can be selected for the lowest isothermal solidification time requirement.

The boridic precipitations in the base metal close to the joint interface area produce brittleness and decrease the formability of the joint. In order to obtain superior mechanical properties, it is necessary to dissolve these borides or to dilute them to a degree where they have no or minimum negative effects. Solid solution in the joint gap with no or minimum precipitates in the base metals would form an ideal TLP bonded joint. Homogenization heat treatment after complete isothermal solidification can be used to achieve comparable properties between the base and filler alloys.

Higher bonding temperature reduces the isothermal solidification time significantly. However, the change of mechanical properties of the base metal should be carefully studied before increasing the temperature.

Finally, efforts should be continued in developing a comprehensive mathematical model that accounts for all the different stages of TLP bonding, namely, dissolution of the base metal, liquid homogenization, isothermal solidification and homogenization, and to couple the model with computational thermodynamics in order to predict the final joint microstructure.

References:

1. W. Chen, M.C. Chaturvedi and N.L. Richards: "Effect of Boron Segregation at Grain Boundaries on Heat-Affected Zone (HAZ) Cracking in Wrought Inconel 718", *Metallurgical and Materials Transactions A,* Vol. 32, No. 4, 2001, 931-939.

2. O.A. Ojo, N.L. Richards and M.C. Chaturvedi: "Isothermal Solidification During Transient Liquid Phase Bonding of Inconel 738 Superalloy", *Science and Technology of Welding and Joining*, Vol. 9, No. 6, 2004, 532-540.

3. J.A. Penso, Y.M. Lattarulo, A.J. Seijas, J. Torres, D. Howden and C.L. Tsai: "Understanding Failure Mechanism to Improve Reliability of Coke Drums", *ASME Pressure Vessel and Piping Division Publication,* Vol. 395, 1999, 243-253.

4. M.T. Cabrillat, P. Allegre, E. Pluyette and B. Michel: "Intergranular Reheat Cracking in 304H Components. Experiments and Damage Evaluation", *Transactions SMiRT,* Vol. 16, Washington DC, August, 2001, 1-8.

5. M. Chabaud-Reytier, L. Allais, D. Poquillon, C. Caes-Hogrel, M. Mottot and A. Pineau: "Modelling Creep Damage in Heat Affected Zone in 321 Stainless Steel. Part I: Quantitative Study of Intergranular Damage", *Materials at High Temperatures* (UK), Vol. 18, No. 2, 2001, 71-80.

6. S.K. Tung, L.C. Lim and M.O. Lai:"Solidification Phenomena in Nickel Base Brazes Containing Boron and Silicon", *Scripta Materialia,* Vol. 34, 1996, 763-769.

7. A. Sakamoto, C. Fujiwara, T. Hattori and S. Sakai: "Optimizing Processing Variables in High-Temperature Brazing with Nickel-Based Filler Metals", *Welding Journal,* Vol. 68, No. 3, 1989, 63-71.

8. E.P. Degarmo, J.T. Black and R.A. Kohser: "Materials and process in manufacturing", John Wiley and Sons, USA, 2003, pp. 974.

9. M. Schwartz: "Brazing", ASM International, USA, 1987, pp. 1-37 and 189-268.

10. S.L. Feldbauer: "Modern brazing of stainless steels", *Welding Journal*, Vol. 83, No.10, 2004, 30-32

11. D.M. Jacobson and G. Humpston: "Principles of Brazing", ASM International, Ohio, USA, 2005, pp. 207.

12. http://www.wallcolmonoy.com/TechServices/NicrobrazNews.htm, "*Nicrobraz Technical Articles Library*," Wall Colmonoy Corporation, USA.

13. T.B. Massalaski: "Binary alloy phase diagrams", ASM International, Metals Park, OH, 1986.

14. E. Lugscheider and K.D. Partz: "High temperature brazing of stainless steel with nickel-base filler metals BNi-2, BNi-5 and BNi-7", *Welding Journal*, Vol. 62, No. 6, 1983, 160s-164s.

15. Y. Natsume, K. Ohsasa and T. Narita: "Phase field simulation of transient liquid phase bonding process of Ni using Ni-P binary filler metal", *Materials Transactions*, Vol. 44, No. 5, 2003, 819-823.

16. S.C. DuBois: "Braze filler metal with enhanced corrosion resistance", United States Patent, No. 5,183,636, February, 1993.

17. B. Zorc and L. Kosec: "Comparison of Brazed Joints made with BNi-1 and BNi-7 Nickel-base Brazing Alloys", *Revista de Metalurgia*, Vol. 36, No. 2, 2000, 100-107.

18. B. Rhee, S. Roh and D. Kim: "Transient Liquid Phase Bonding of Nitrogen Containing Duplex Stainless Steels", *Materials Transactions,* Vol. 44, No. 5, 2003, 1014-1023.

19. M.M. Mcdonald, D.L. Keller, C.R. Heiple and W.E. Hofmann: "Wettability of brazing filler metals on molybdenum and TZM", *Welding Journal*, Vol. 68, No. 10, 1989, 389s-395s.

20. A. Robinkin and N.J. DeCristofaro: "Iron-chromium base brazing filler metals", United States Patent, No. 6,883,701, April, 2005.

21. W.F. Gale and D.A. Butts: "Transient Liquid Phase Bonding", *Science and Technology of Welding and Joining*, Vol. 9, No. 4, 2004, 283 – 300.

22. J.C. Ambrose, S. Jenkins and M.G. Nicholas: "Some effects of composition and surface preparation on the wetting behavior of nickel base brazes", *Brazing and Soldering*, No. 14, Spring, 1998, 30-33.

23. W.F. Gale and E.R. Wallach: "Wettability of nickel alloys by boron containing brazes", *Welding Research*, 1991 (March), 76s-79s.

24. A. Sakamoto: "Wetting in vacuum inert gas partial pressure atmosphere", *Welding Journal*, Vol. 62, No. 10, 1983, 272s-281s.

25. T.I. Khan, M.J. Kabir and R. Bulpett: "Effect of Transient Liquid Phase Bonding Variables on the Properties of a Micro-Duplex Stainless Steel", *Materials Science and Engineering A*, Vol. 372, 2004, 290-295.

26. O.A. Ojo: "The effects of brazing parameters on microstructure and properties of diffusion brazed joint of IN-738 superalloy", M.Sc. Dissertation, University of Manitoba, 2002.

27. O.A. Ojo, N.L. Richards and M.C. Charturvedi: "Effect of Gap Size and Process Parameters on Diffusion Brazing of Inconel 738", *Science and Technology of Welding and Joining*, Vol. 9, 2004, 209-220.

28. K. Nishimoto, K. Saida, D. Kim and Y. Nakao: "Transient Liquid Phase Bonding of Ni-Base Single Crystal Superalloys", *ISIJ International*, Vol. 35, No. 10, 1995, 1298-1306.

29. X.P. Zhang, Y.W. Shi: "A dissolution model of base metal in liquid brazing filler metal during high temperature brazing", *Scripta Materialia*, Vol. 50, 2004, 1003-1006.

30. X. Wu, R.S. Chandel and H. Li: "Evaluation of Transient Liquid Phase Bonding between Nickel Based Superalloys", *Journal of Materials Science*, Vol. 36, 2001, 1539-1546.

31. R.K. Shiue, S.K. Wu and C.M. Hung: "Infrared repair brazing of 403 stainless steel with a nickel-based braze alloy", *Metallurgical and Materials Transactions A*, Vol. 33, 2002, 1765-1773.

32. R. Spinat and Y. Honnorat: "High Temperature Alloys for Gas Turbines and Other Applications", Reidel Publication Corporation, Dordrecht, Holland, 1986, pp. 151 – 174

33. B. Jahnke and G. Dannhauser: "High Temperature Alloys for Gas Turbines and Other Applications", Reidel Publication Corporation, Dordrecht, Holland, 1986, pp. 175 – 216.

34. J.S.C. Jang and H.P. Shih: "Evolution of Microstructure of AISI 304 Stainless Steel Joint Brazed by Mechanically Alloyed Nickel Base Filler with Different Silicon Content", *Journal of Material Science Letters*, Vol. 22, 2003, 79-82.

35. C.E. Campbell and W.J. Boettinger: "Transient Liquid-Phase Bonding in the Ni-Al-B System", *Metallurgical and Materials Transactions A*, Vol. 31, 2000, 2835-2847.

36. W.F. Gale: "Transient Liquid Phase Bonding of Intermetallic Compounds", *Materials Science Forum*, Vol. 426-432, 2003, 1891-1896.

37. C.E. Campbell and U.R. Kattner: "A thermodynamic assessment of the Ni-Al-B system", Journal of Phase Equilibria, Vol. 20, No. 5, 1999, 485-496.

38. E. Lugscheider, T. Schittny and E. Halmoy: "Metallurgical Aspects of Additive Aided Wide Clearance Brazing with Nickel Based Filler Metals", *Welding Journal*, Vol. 68, No. 1, 1989, 9s – 13s.

39. Y. Nakao, K. Nishimoto, K. Shinozaki and C.Y. Kang: "Joining of Advanced Materials", Chapman and Hall, London, 1990, pp. 129-144,

40. E.R. Mandrell and E.R. Wallach: "Recent Trends in Welding Science and Technology", ASM International, Materials Park, OH, 1990.

41. S.V. Orel, L. Parous and W.F. Gale: "Diffusion Brazing of Nickel Aluminides", *Welding Journal*, Vol. 74, No. 9, 1995, 319s-324s.

42. R. Thamburaj, W. Wallace and J.A. Goldak: "Post Weld Heat Treatment Cracking in Superalloys", *International Materials Reviews*, Vol. 28, No. 1, 1983, 1-22.

43. Y. Zhou, W.F. Gale and T.H. North: "Modeling of Transient Liquid Phase Bonding", *International Materials Reviews*, Vol. 40, No. 5, 1995, 181-196.

44. D.S. Duvall, W.A. Owczarski. And D.F. Paulonis: "TLP Bonding: New Method for Joining Heat Resistant Alloys", *Welding Journal*, Vol. 53, No. 4, 1974, 203-214

45. G.S. Hoppin and T.F. Berry: "Strain-Age Characteristics in Welded Rene 41-Phase II", *Welding Journal*, Vol. 48, No. 11, 1969, 505s-509s.

46. H. Ikawa, Y. Nakao and T. Isai: "Research Theoretical Considerations on the Metallurgical Process in TLP Bonding of Nickel-Base Superalloy", *Transactions of Japan Welding Society*, Vol. 10, No. 1, 1979, 24-29.

47. D.S. Duvall, W.A. Owczarski, D.F. Paulonis, and W.H. King: "Methods of Diffusion Welding the Superalloy Udimet 700", *Welding Journal*, Vol. 49, No. 2, 1972, 41s-49s.

48. B. Jahnke and J. Demny: "Microstructural Investigations of a Nickel-based Repair Coating Processed by Liquid Phase Diffusion Sintering", *Thin Solid Films*, Vol. 110, No. 3, 1983, 225-235.

49. T.J. Moore and T.K. Glasgow: "Diffusion Welding of MA 6000 and a Conventional Nickel-Base Superalloy", *Welding Journal*, Vol. 64, No. 8, 1985, 219s-226s.

50. G.E. Sheward: "High Temperature Brazing in Controlled Atmosphere", Pergamon Press, London, 1985.

51. A. Suzamura, T. Onzawa, and H. Tamura: "Effects of Using Amorphous Interlayers on Liquid Phase Diffusion Welding Process", *Quarterly Journal of Japan Welding Society*, Vol. 3, No. 2, 1985, 321-327.

52. Y. Nakao, K. Nishimoto, K. Shinozaki, K.C. Yun and Y. Hori: "Study on Transient Liquid Insert Metal Diffusion Bonding of Nickel Base Superalloys. I. Dissolution Phenomenon of Base Metal into Liquid Insert Metal", *Quarterly Journal of Japan Welding Society*, Vol. 6, No. 4, 1988, 67-74.

53. Y. Nakao, K. Nishimoto, K. Shinozaki and C.Y. Kang: "Theoretical Research on Transient Liquid Insert Metal Diffusion Bonding of Nickel Base Alloys", Proceedings of the Sixth International Symposium on Superalloys, Chamption, Pennsylvania, September 18-22, 1988, pp. 775-784.

54. A. Rabinkin: "New Applications for Rapidly Solidified Brazing Foils", *Welding Journal*, Vol. 68, No. 10, 1989, 39-46.

55. Y. Nakao and K. Shinozaki: "Transient Liquid Phase Diffusion Bonding of Iron Base Oxide Dispersion Strengthened Alloy MA 956", *Materials Science and Technology*, Vol. 11, No. 3, 1995, 304-311.

56. K.C. Wu: "Resistance NOR-Ti-BOND Joining of Titanium Shapes", *Welding Journal*, Vol. 49, No. 9, 1971, 386s-393s.

57. R.R. Wells: "Microstructural Control of Thin Film Diffusion Brazed Titanium", *Welding Journal*, Vol. 55, No. 1, 1976, 20s-27s.

58. B. Norris: "Designing with Titanium", The Institute of Metals, London, 1986, pp. 83-86.

59. T. Funamoto, R. Kaziwara, M. Kato, T. Matsuzaka and T. Shida: "Study on Liquid Phase Diffusion Welding of Aluminum with Alloyed Film with Sputtering", *Quarterly Journal of Japan Welding Society*, Vol. 5, No. 4, 1987, 3-9.

60. J.T. Niemann and R.A. Garret: "Eutectic Bonding of Boron-Aluminum Structural Components", *Welding Journal*, Vol. 52, No. 4, 1974, 175-184.

61. T. Onzawa, A. Suzamura and J.H. Kim: "Relation Between Reaction Zone Thickness and Tensile Strength in Titanium Matrix Composites Reinforced with SiC Fibers", *Quarterly Journal of Japan Welding Society* , Vol. 8, No. 4, 1990, 74-78.

62. T. Onzawa, A. Suzamura and J.H. Kim: "Filament/Matrix Interaction if Titanium-Matrix Composites Reinforced with SiC Fibers", *Quarterly Journal of Japan Welding Society*, Vol. 8, No. 2, 1990, 122-128.

63. Z. Li, W. Fearis and T.H. North: "Particulate Segregation and Mechanical Properties in Transient Liquid Phase Bonded Metal Matrix Composites", *Materials Science and Technology*, Vol. 11, No. 4, 1995, 363-369.

64. T. Funamoto, H. Wachi and R. Kaziwara "Study on Liquid Diffusion Welding of Copper to Austenitic Stainless Steel Using Cu-Ti Thin Alloyed Layer Deposited by Sputtering", *Quarterly Journal of Japan Welding Society*, Vol. 6, No. 2, 1988, 23-29.

65. L. Bernstein and H. Bartholomew: "Applications of Solid-Liquid Interdiffusion (SLID) Bonding in Integrated Circuit Fabrications", *Transactions of AIME*, Vol. 236, No. 3, 1966, 405-412.

66. R.E. Loehmann: "Surfaces and Interfaces in Ceramic and Ceramic-Metal Systems", (ed. J. Pask and A. Evans), Plenum Press, New York, 1980, pp. 701-711.

67. G.V. Samsonov (ed.): "Handbook of the Thermophysical Properties of the Elements", Oldbourne, London, UK, 1968.

68. D.R. Lide (ed.): "CRC Handbook of Chemistry and Physics", 83rd edn., CRC Press, Boca Raton, FL, USA, 2002.

69. E. Lugscheider, O. Knotek and K. Klohn: "Melting Behavior of Nickel-Chromium-Silicon Alloys", *Thermochemica Acta*, Vol. 29, No. 2, 1979, 323-326.

70. G.E. Sheward and G.R. Bell: "Development and Evaluation of a Nickel-Chromium-Phosphorus Brazing Filler Metal", *Welding Journal*, Vol. 55, No. 10, 1976, 285s-292s.

71. E. Lugscheider, K.D. Partz and R. Lison: "Thermal and Metallurgical Influences on AISI 316 and Inconel 625 by High Temperature Brazing with Nickel-Base Filler Metals", *Welding Journal*, Vol. 61, No. 10, 1982, 329s-333s.

72. E. Lugscheider and H. Pelster: "Nickel based Filler Metals of Low Precious Metal Content", *Welding Journal*, Vol. 62, No. 10, 1983, 261s-266s.

73. A. Rabinkin: Proc. British Association for Brazing and Soldering, Preprint, 1988.

74. F.P.L. Kavishe, S.J. Barnes and T.J. Baker: Proc. British Association for Brazing and Soldering, Preprint, 1988.

75. E. Lugscheider and H. Krappitz: "The Influence of Brazing Conditions on the Impact Strength of High Temperature Brazed Joints", *Welding Journal*, Vol. 65, No. 10, 1986, 261s-267s.

76. V. Ruza: "The Impact of Brazed Joints in High Strength Steels", *Metal Construction*, Vol. 11, No. 11, 1979, 600-602.

77. R. Holis and A.L. Walker: *Metallurgia*, 1969, 79, 89-92 [Cited in 22]

78. A.G. Ward and J.W. Taylor: "Dynamic Solution Rate Studies of Solid Metals in Liquid Metals", *Journal of Institute of Metals*, Vol. 86, 1957, 36-42 [Cited in 21].

79. E.A. Brandes and G.B. Brook (eds.): "Smithells Metals Reference Book", 7th Edition, Butterworth-Heinemann, Oxford, UK, 1992 [Cited in 21].

80. J.T. Niemann and R.A. Garret: "Eutectic Bonding of Boron-Aluminum Structural Components", *Welding Journal*, Vol. 52, 1974, 175-184.

81. W.D. MacDonald and T.W. Eager: "Transient Liquid Phase Bonding", *Annual Review of Materials Science*, Vol. 22, 1992, 23-46.

82. H. Nakagawa, C.H. Lee and T.H. North: "Modeling of Base Metal Dissolution Behavior during Transient Liquid Phase Bonding", *Metallurgical and Materials Transactions A*, Vol. 22, 1991, 543-555.

83. I. Tuah-Poku, M. Dollar and T.B. Massalski: "A study of the transient liquid phase bonding process applied to a silver/copper/silver sandwich joint", *Metallurgical and Materials Transactions A*, Vol. 19, 1988, 675-686.

84. J.S. Langer and R.F. Sekerka: "Theory of Departure from Local Equilibrium at the Interface of a Two Phase Diffusion Couple", *Acta Metallurgica*, Vol. 23, No. 10, 1975, 1225-1237.

85. E.A. Moelwyn-Hughes: "The Kinetics of Reaction in Solution", Clarredon Press, Oxford, UK, 1947, p. 374.

86. S. Liu, D.L. Olson, G.P. martin and G.R. Edwards: "Modeling of Brazing Processes that Use of Coatings and Interlayers", *Welding Journal*, Vol. 70, No. 8, 1991, 207s-215s.

87. Y. Nakao, K. Nishimoto, K. Shinozaki and K.C. Yun: "Analysis of Isothermal Solidification Process of Transient Liquid Insert Metal Diffusion Bonding. II. Study on Transient Liquid Insert Metal Diffusion Bonding of Nickel Base Superalloys", *Quarterly Journal of Japan Welding Society*, Vol. 7, No. 2, 1989, 47-53.

88. Y. Zhou: "Analytical Modeling of Isothermal Solidification during Transient Liquid Phase Bonding (TLP) Bonding", *Journal of Materials Science Letters*, Vol. 20, 2001, 841-844

89. Y. Nakao, K. Nishimoto, K. Shinozaki and C.Y. Kang: ibid, 1989, p. 60. [Cited in 88]

90. C.H. Lee, T.H. North and H. Nakagawa, "Isothermal Solidification During TLP-Brazing (Modeling and Experimental Justification)", Proceedings of the 71st American Welding Society Convention, Anaheim, CA, 1990, pp. 243-246.

91. J. Crank: "The Mathematics of Diffusion", 2nd ed., Oxford University Press, Oxford, UK, 1975.

92. W.F. Gale and E.R. Wallach: "Microstructural Development in Transient Liquid Phase Bonding", *Metallurgical and Materials Transactions A*, Vol. 22, No. 10, 1991, 2451-2457.

93. G. Lesoult: Center for Joining of Materials Report, Carnegie Mellon University, Pittsburgh, PA, Sept. 1976.

94. P.V. Danckwerts: "Unsteady State Diffusion or Heat Conduction with Moving Boundary", *Transactions of Faraday Society*, Vol. 46, 1950, 701-712.

95. J.E. Ramirez and S. Liu: "Diffusion Brazing in the Nickel-Boron System", *Welding Research*, Vol. 71, No. 10, 1992, 365s-375s. for 1358K bonding temperature and 70 μm joint gap

96. Y. Zhou: "Numerical Modeling of Process Kinetics during TLP Bonding and Other Diffusion Controlled Processes", Ph.D. Dissertation, University of Toronto, 1994.

97. P. Shewmon: "Diffusion in solids", 2nd ed., Minerals, Metals and Materials Society, Warrendale, PA, USA, 1989.

98. K.N. Dimou and E.E. Adams: "A Random Walk Particle Tracking Model for Well-Mixed Estuaries and Coastal Waters", *Estuaries and Coastal Shelf Series*, Vol. 37, 1993, 99-110.

99. V. Nassehi and S. Passone: "Testing Accuracy of Finite Element and Random Walk Schemes in Prediction of Pollutant Dispersion in Coastal Waters", *Environmental Fluid Mechanics*, Vol. 5, 2005, 199-214.

100. A.W. Visser: "Using Random Walk Models to Simulate the Vertical Distribution of Particles in a Turbulent Water Column", *Marine Ecology Progress Series*, Vol. 158, 1997, 275-281.

101. C.F. Scott: "Particle Tracking Simulation of Pollutant Discharges", *Journal of Environmental Engineering*, Vol. 123, 1997, 919-927.

102. A.M. Riddle: "Investigations of Model and Parameter Uncertainty in Water Quality Models Using a Random Walk Method", *Journal of Marine Systems*, Vol. 28, 2001, 269-279.

103. A.M. Riddle, E.M. Beling, R.J. Murray-Smith: "Modeling the Uncertainties in Predicting Produced Water Concentrations", *Environmental Modeling and Software*, Vol. 16, 2001, 659-668.

104. T. Tokunaga, K. Nishio, H. Ohtani and M. Hasebe: "Phase equilibria in the Ni-Si-B system", *Materials Transactions*, Vol. 44, 2003, 1651-1654.

105. P. Villars, A. Prince and H. Okamoto: "Handbook of Ternary Alloy Phase Diagrams", ASM International, Materials Park, OH, USA, 1995, 5508-5513.

106. S. Taylor: "Grade 321", *Stainless Steel Industry*, Vol. 26, No. 154, 1998, 2-4.

107. Y.E. Gol'dshtein and V.G. Mizin: "Some Peculiarities of the Structure of High Boron Steels", *Metal Science and Heat Treatment*, Vol. 30, No. 7, 1988, 479-484.

108. K. Ohsasa, T. Shinmura and T. Narita: "Numerical modeling of the transient liquid phase bonding process of Ni using Ni-B-Cr ternary filler metal", *Journal of Phase* Equilibria and Diffusion, Vol. 20, No. 3, 1999, 199-206.

109. B. Predel: "Phase Equilibria, Crystallographic Data and Values of Thermodynamic Properties of Binary Alloys: Group IV: Physical Chemistry", Springler-Verlag Berlin and Heidelberg, Germany, 1992, pp. 1-75.